

Title	液体電極プラズマ発光分光分析法を用いた長期間測定のための方法
Author(s)	Ruengpirasiri, Prasongporn
Citation	
Issue Date	2019-09
Type	Thesis or Dissertation
Text version	ETD
URL	http://hdl.handle.net/10119/16191
Rights	
Description	Supervisor:高村 禪, 先端科学技術研究科, 博士

**Methods for Long Time Monitoring Using
Liquid Electrode Plasma
Optical Emission Spectrometry**

Prasongporn RUENGPIRASIRI

Japan Advanced Institute of Science and Technology

Doctoral Dissertation

**Methods for Long Time Monitoring Using
Liquid Electrode Plasma
Optical Emission Spectrometry**

Prasongporn RUENGPISIRI

Supervisor: Professor Yuzuru Takamura

Graduate School of Advanced Science and Technology

Japan Advanced Institute of Science and Technology

Materials Science

September 2019

Abstract

Liquid electrode plasma (LEP) driven by alternating current (AC) is used as an excitation source for elemental analysis. LEP forms in a vapor bubble generated inside a narrow-center microchannel by using high-voltage power. This technique can detect metals with high sensitivity and high selectivity. More recently, we found the better conditions to generate LEP by alternating current with higher stability and significantly low damages on microchannel, called the new method as AC-LEP. In this plasma, an air bubble remained in the LEP channel during plasma generation by AC power source. The bubble is expected to affect plasma generation strongly. In order to investigate in detail the effect of the bubbles, we fabricated a microfluidic system to introduce different kinds of gas bubbles intentionally into the LEP channel.

In AC-LEP, significantly less channel damage (1/3000) was reported compared to direct current LEP (DC-LEP). However, the mechanism has not been clear. In this paper, the effects of external gas introduction into AC-LEP and DC-LEP were studied. The results showed that the external gas bubbles facilitated stable and highly sensitive plasma generation with lower power, reducing channel damage and increasing the lifetime of the analysis chip. These effects are significant in Ar introduction and AC-LEP cases. The facts suggest that the lower damage in conventional AC-LEP without gas introduction is attributed to H₂/O₂ bubbles generated by hydrolysis at electrodes and consequently introduced into the LEP from outside of narrow channel.

In order to increase detection efficiency, electrochemistry is one of an attractive method for preconcentration of heavy metal. Depending on the nature of analytes and sample matrix, electrochemical detection (ECD) is very sensitive and can be detected in the femtomole/L (10⁻¹⁵ M) range. In this work, the combination of two techniques for heavy metal detection was studied. A more chemical-specific detection condition can be acquired by selecting the suitable applied voltage for the oxidation and reduction potential and working electrode materials. Target compounds (analytes) are separated using a specific voltage in reduction reaction process. After separation, the compounds present at working electrode will be directly desorption and detection by using LEP.

Keywords: Liquid electrode plasma, Electrodeposition, Elemental analysis

Acknowledgements

First of all, I would like to express my deepest gratitude and appreciation to my advisor, *Professor Yuzuru Takamura* and *Professor Phan Trong Tue* for generous supervision, precious guidance, suggestions and continuous encouragement throughout this research work. I am also deeply sincerest to *Professor Masahiko Tomitori*, *Professor Goro Mizutani*, *Associate Professor Yuichi Hiratsuka*, and *Professor Hiroshi Hasegawa* from, Kanazawa University, my thesis committee members, for giving valuable comments and advice. Moreover, Acknowledgements are extended to all members of Takamura Laboratory at School of Materials Science (JAIST) for their helpful and comments during the research work.

The author would like to thank *Dr. Tamotsu Yamamoto*, CEO of Micro Emission Ltd., *Mr. Syuji Tatsumi*, and *Ms. Jun Mimami* of Micro Emission Ltd. for their instrumentation, kindly help and precious suggestion along with this research.

Special thanks are extended to my advisor for minor research, *Professor Hiroshi Hasegawa* from Faculty of Chemistry, Institute of Science and Engineering, Kanazawa University, for providing a great opportunity, knowledge and laboratory under his supervision. I would like to express my gratitude to *Mr. Suman Barua* and *Ms. Maho Miyaguchi* for supporting me all the time I spent in Hasegawa Laboratory, Kanazawa University.

Finally, I am especially affectionately thankful to my parents and family for their heartfelt unlimited support, tender love, continual care, enthusiasm support and invaluable encouragement during study in the Ph.D. program. My special thanks are extended to everyone who helped me to succeed in this dissertation during my time at Japan Advanced Institute of Science and Technology.

Autumn 2019

Prasongporn Ruengpirasiri

Contents

	Pages
Abstract.....	I
Acknowledgements.....	II
CHAPTER I GENERAL INFORMATION	1
1.1 Introduction of plasma and liquid plasma source for elemental analysis	1
1.1.1 Electrolyte cathode discharge atomic emission spectrometry (ELCAD-AES).....	3
1.1.2 Liquid cathode glow discharge (LCGD).....	5
1.1.3 Solution-cathode glow discharge (SCGD).....	6
1.1.4 Dielectric barrier discharge (DBD).....	7
1.2 Introduction of liquid electrode plasma (LEP) optical emission spectrometry and principle of LEP	8
1.3 Introduction of heavy metal contamination	11
1.4 Introduction of electrochemistry and its applications	12
1.5 Purpose and outlines.....	14
1.6 Dissertation organization.....	15
1.7 References	16
CHAPTER II DEVELOPMENT OF THE LIQUID ELECTRODE PLASMA (LEP) CHIP WITH GAS INTRODUCTION.....	22
2.1 Introduction	22
2.2 Fabrication of new microchip design including gas channel	24
2.3 Optimization of experimental parameters	29
2.3.1 Liquid and gas channel size	29
2.3.2 Gas flow rate	29
2.3.3 Types of gases	32

CHAPTER III STUDY ON EFFECT OF INTRODUCED GAS BUBBLES FOR THE LOW CHANNEL DAMAGE IN DIRECT AND ALTERNATING CURRENT LIQUID ELECTRODE PLASMA ATOMIC EMISSION SPECTROMETRY	38
3.1 Introduction	38
3.2 Optimization of experimental condition for fair comparison of channel expansion	42
3.3 Channel damage comparison	44
3.4 Investigation of effects of gas introduction.....	47
3.5 Long time stability of AC-LEP emission signal with various gases.....	52
3.6 Measurement of excitation temperature and effects of introduced gases on excitation temperature.....	53
3.7 Analytical performance of AC-LEP.....	57
3.8 Conclusion.....	58
CHAPTER IV METHOD DEVELOPMENT OF HEAVY METAL DETECTION BY ELECTRODEPOSITION COUPLED WITH LEP-OES	62
4.1 Introduction	62
4.2 Design of microchip for new detection system.....	64
4.3 Characterization of electrodeposition coupled with LEP-OES.....	65
4.4 Optimization of experimental conditions.....	67
4.6 Conclusion.....	81
4.7 References	82
CHAPTER V GENERAL CONCLUSION	86
LIST OF PUBLICATIONS	88

CHAPTER I

GENERAL INFORMATION

1.1 Introduction of plasma and liquid plasma source for elemental analysis

Irving Langmuir (1928) first introduced the term “plasma” to describe a state that contains balanced charges of ions and electrons that make it electro-conductive. Plasma can be considered as one of the four fundamental states of matter, together with liquids, solids, and gases. Plasma is a state of matter where gas phase is activated until electrons inside atom are no longer connected with any particular atomic nucleus. Plasmas consisted of positively charged ions and unbound electrons. Plasma can be generated by heating gas until it ionized or by subjecting it to a concentrated high electromagnetic field. Plasma is rarely encountered in daily life, while the other three states of matter are common.

The plasma is commonly found on earth, for example, lightning stroke and polar wind. It can exist shortly in the Earth’s atmosphere and can be generated artificially in laboratory and in industry. The applications of laboratory-generated plasma are electronics, lasers, fluorescent lamps, and many others. The main features that attracted many researchers for applications in physics and chemistry are high temperature compared with conventional chemical technique, generation of high energetic and chemically active species (e.g., electrons, ions, and radicals), and providing extremely high concentrations of the chemically active species while keeping bulk temperature as low as room temperature [1].

Electrical discharges in liquids generated plasmas are finding wide applicability in a number of modern technology areas. Many of researchers found that plasmas in liquids produce strongly non-equilibrium plasmas, where the electron temperatures are much larger than the

vapor temperature and the liquid temperature [2]. For elemental analysis in laboratory, plasma is often generated through electrical discharges, including glow discharges, non-thermal atmospheric pressure discharges, arc discharges, and other types of micro-discharges. In the elemental analysis area, the standard laboratory techniques are inductively coupled plasma optical emission spectrometry (ICP OES), inductively coupled plasma mass spectrometry (ICP MS), and atomic absorption spectrometry (AAS). However, these techniques are not feasible for on-site analysis because they require a high power supplier and supporting equipment (especially a nebulizer and carrier gas). Besides, these methods usually require relatively high cost of maintenance and operation, which is not frugality for continuous environmental monitoring. Therefore, the demand of miniaturized plasma sources, which are more adaptable in ion generation, require lower power, and are adequate for on-site administration, is developed. To serve this goal, liquid discharge micro-plasma becomes a good nominee.

Overall, this study has mainly discussed on plasma that is generated by the electrical liquid discharge and is performed as an excitation source for optical detection of heavy metal ions. The generated plasmas are found in a narrow area between a sample solution and an electrode or in between two liquid electrodes by an application of a high and concentrated voltage at the atmospheric pressure. With power from discharge plasmas, the atomic lines of heavy metal ions in the sample solution are obtained in the emission spectrum. Thus, the analyte ions in the solution can be detected qualitatively and quantitatively. The principle of emission spectrum appearance is illustrated in Fig 1.1. Electrons with different energy levels surround a nucleus. Without any external energy, electrons are at ground state of each orbit. Once photons or external electrons through applied energy excite an atom, electrons are moved to the higher energy level, so called excited state. After that, the excited electrons return to the initial state (relaxation), characteristic wavelengths of photons are emitted. The emission light intensity is directly proportional to the amount of the excited atoms thus it is corresponding to

concentration of the analyzed target ions. The fundamental of optical emission spectrometry has been extensively employed for qualitative detection by characteristic wavelengths and quantitative detection by emission spectrum intensity.

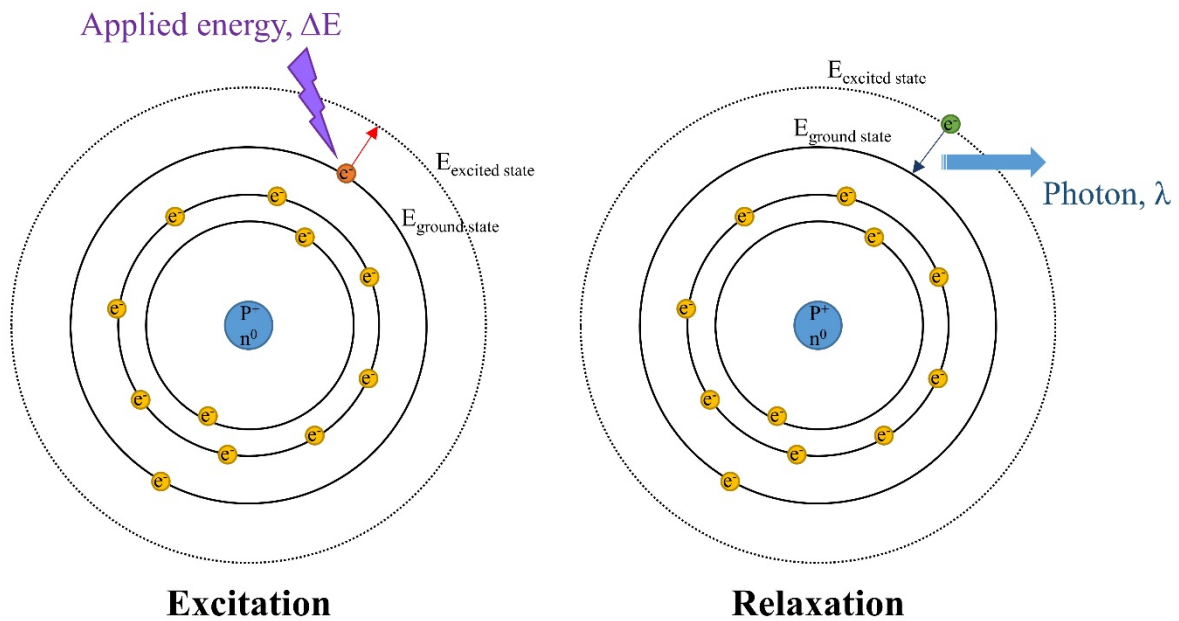


Figure 1.1 Mechanism of photon generation of specific wavelength in optical emission spectrometry.

Various paper reviews [3-5] have also summed up the design of different discharge structures with characteristics and principle processes. Next, some example of typical liquid electrode discharge sources are summarized.

1.1.1 Electrolyte cathode discharge atomic emission spectrometry (ELCAD-AES)

To begin with, electrolyte cathode discharge atomic emission spectrometry, ELCAD-AES, has become an analytical approach for elements determination in sample solution,

though no commercial instrument was available at that time [6]. Since then, many efforts have been made for the development and studies of mechanism of glow discharge electrolysis [7-9]. The phenomenon of electrolysis with metal cathode and glow-plasma anode, the so-called glow discharge electrolysis (GDE) [10]. Cserfalvi et al. investigated that the glow discharge could be appeared between liquid sample surfaces in atmosphere and a metal cathode surfaces; thus, the plasma spectrum incorporated the atomic lines of the metals presented in the sample [11].

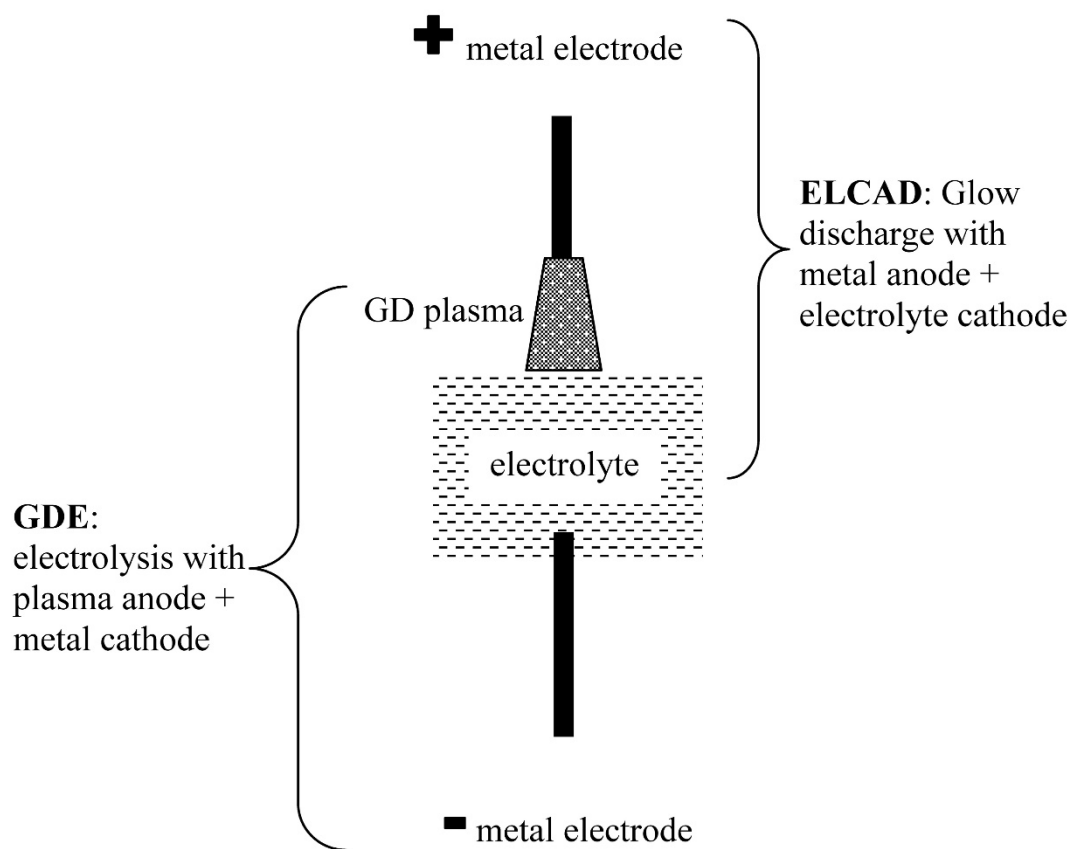


Figure 1.2 Schematic connection and separation of the GDE and the ELCAD concepts.

[Introduced by Mezei et al. ref. 10].

1.1.2 Liquid cathode glow discharge (LCGD)

Recently, a simultaneous detection of trace Cu, Co and Ni in aqueous solution by a liquid cathode glow discharge (LCGD), as a micro-plasma excitation source of atomic emission spectrometry (AES), was established. The detection limit (LOD) of Cu, Co and Ni are 0.380, 0.080, and 0.740 mg L⁻¹, respectively, which are consistent with electrolyte cathode atmospheric glow discharge (ELCAD). Compared with ICP-AES, the LCGD-AES is compact in size, small power consumption, no inert gas requirement and relatively cheap in set-up. This showed a feasibility method as a portable instrument for on-site and real-time monitoring of elemental in sample solutions, as shown in Fig 1.3 [12].

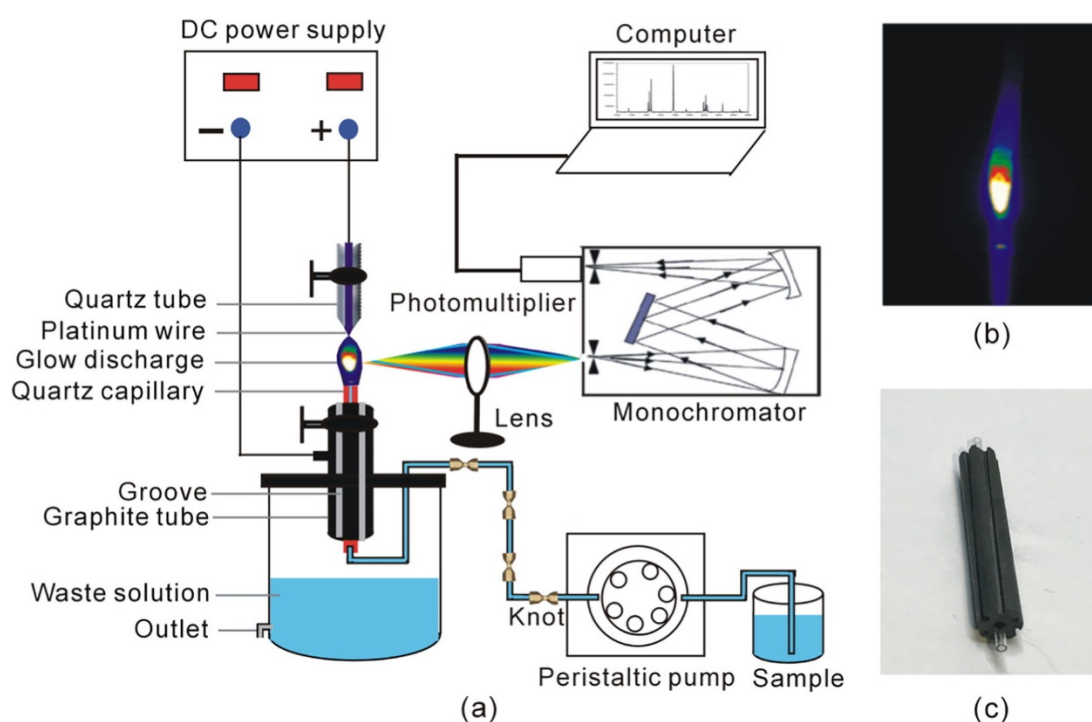


Figure 1.3 Schematic diagram of the experiment setup for LCGD-AES system ((a): the experiment setup for LCGD-AES, (b): the photograph of glow discharge plasma at 640 V, (c): the photograph of graphite tube). [Introduced by Yu et al. ref. 12]

1.1.3 Solution-cathode glow discharge (SCGD)

Webb et al. early introduced the simplified ELCAD design, which they called as solution-cathode glow discharge (SCGD) [13, 14]. In the solution cathode discharge system, solution is the cathode while a metal electrode is served as the anode. Gas is ionized when a high voltage is applied between the two electrodes, then plasmas appear. After that, volatilization of sample solution take place and the dissolved elements in solution will enter the plasma, followed by atomization and excitation of ions. Thus, the characteristic emission spectrum is finally collected. Under the optimized parameters and conditions, the limit of detection (LOD) was 0.032 mg L^{-1} calculated by $3\text{SDBLANK}/k$ ($n = 11$) [15]. Another advantage of SCGD is that it can be operated in an atmospheric pressure with relatively good performance and detection system. Other reported that detection limits for elemental species found in the range of 0.1 to 4 ppb. The linear dynamic range spanned more than 4 orders and the precision varied between 5 and 16% of relative standard deviation [16].

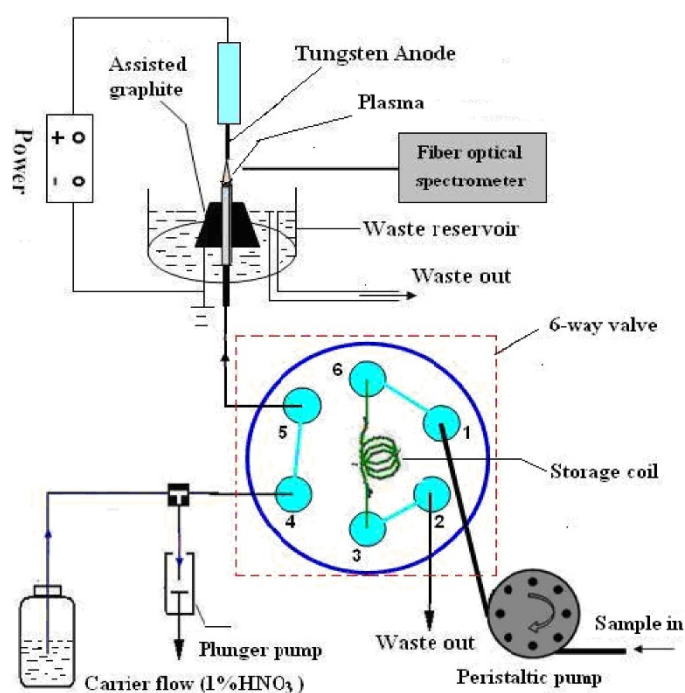


Figure 1.4 The configuration of the SCGD-atomic emission spectrometry device. [Introduced by Zu et al. ref. 15]

1.1.4 Dielectric barrier discharge (DBD)

Dielectric barrier discharge (DBD) is a common non-thermal plasma, which was first introduced by Miclea et al. [17]. The electrical discharge progressed due to high voltage in the narrow area between two electrodes, and at least one of them is covered with a dielectric. Typical planar DBD configurations are illustrated in Fig. 1.5. Because of the presence of at least one dielectric barrier, these discharges require alternating voltages for their operation [18]. Other reports of DBD can be found in the ref. [5, 19, 20].

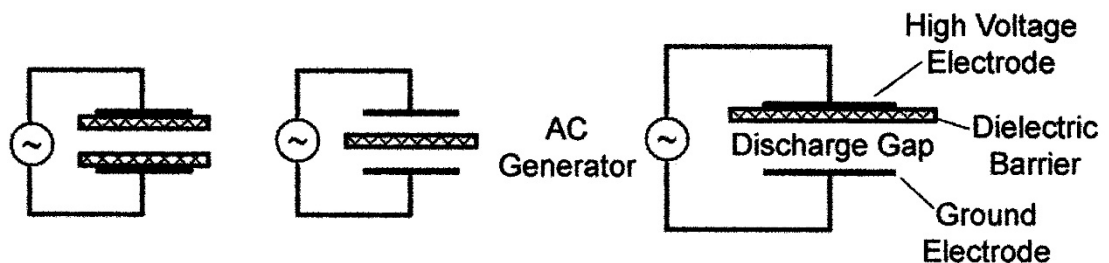


Figure 1.5 Basic dielectric-barrier discharge configurations. [Introduced by Kogelschatz et al. ref. 18]

Liquid electrode discharge micro plasma provides a low-cost, compact platform for quick and direct scrutiny of metal ions in aqueous samples because of no carrier gases required for plasma generation. The integration of liquid electrode discharge to other microfluidics systems has been realized.

1.2 Introduction of liquid electrode plasma (LEP) optical emission spectrometry and principle of LEP

Liquid electrode plasma (LEP) has a short history from its study to applications when compared with the other micro plasma sources for elemental analysis. This novel method allows miniaturizing plasma excitation source, and requires neither high power source nor carrier gas. Therefore, device using LEP can be made compact and portable. Iiduka et al. first introduced LEP-AES in 2004 [21]. LEP has been utilized as an alternative excitation source for the qualitative and quantitative analysis of various elements through their atomic emission spectrometry (AES). The channel of microchip is made narrower in between its two ends and contains electrolyte solution. When a voltage pulse is applied to two electrodes at both ends of the micro channel, concentrated electric current generates Joules heating and then water vapor bubble is formed. Inside of generated bubble, micro plasma is appeared from the electrical discharge. Elements in sample solution enter the plasma and emit their specific spectra that are recorded by spectrometer. The principle of LEP is presented in Fig. 1.6. LEP is as sensitive as conventional AES methods [22] and requires no plasma gas, low power source, and very small sample usage. Thus, it is useful not only for elemental analysis but also for other high sensitive applications by using specific element as a label [23].

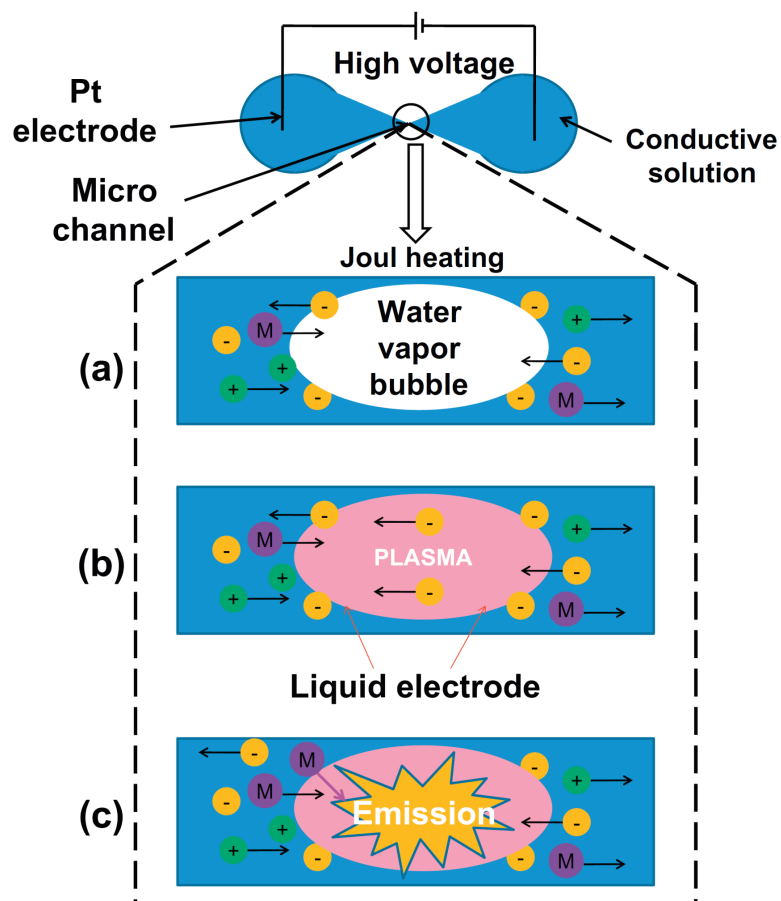


Figure 1.6 Principle of LEP-AES. A water bubble is generated at the center (a). Subsequently, plasma occurs in the bubble (b). Elements in sample solution enter the plasma and emit their specific spectra (c). Using an Atomic emission spectrometer, elements can be detected (qualitatively and quantitatively). [Introduced by Khoai et al. ref. [24]]

From our reported research [24-26], some advantages of the method are proven: high sensitivity, no trained personnel required, low background and small sample amount [27] (40 μL for a single measurement). Importantly, LEP-AES does not require supportive gas or nebulizer and it can be battery-operated. The last two specifications enable the LEP-based handheld device. Fig. 1.7 illustrates an ultra-compact elemental analyzer MH-5000 that has been developed by Micro Emission Ltd with some features.



Figure 1.7 An ultra-compact elemental analyzer MH-5000. (Source: <http://www.micro-emission.com/>)

In previous works, LEP was driven by a direct current (DC) source, where the width of narrow channel after the number of repeated measurements was apparently larger than that before the measurements by approximately 1.5 times [22]. This is due to plasma damage. Currently, the channel damage is a big issue that makes short chip lifetime and increase cost of operation, especially for continuous elemental analysis. For DC-LEP, the water bubble size is increased and then bubble interfered the electric flow, lastly the plasma stops [28]. In contrast, the video recorded by high-speed camera also showed that an gas bubble remained in the liquid narrow channel during plasma generation by alternating current (AC) power source. Because of applied voltage, the bubble expands and plasma appears inside the bubble, after that bubble returned to shrink form. From these above observations, alternating current-LEP (AC-LEP) looks to relieve channel damage very much [28], but the factors and mechanism of this

improvement is not clear. Therefore, it becomes more interesting to investigate in detail about the generated bubbles of plasma generation with AC power source.

To sum up, LEP-OES is a novel liquid discharge based analytical technique extraordinarily sensitive with metals. Advantages of LEP-OES are low power consumed, portable, small sample usage and ease of operation. In addition, the sensitivity of the method can be improved by integration with other preconcentration technique, for instance, electro deposition. With this approach, concentration of target analyte was sufficiently high to be measurable. Finally, the sensitivity of LEP integrated method was improved.

1.3 Introduction of heavy metal contamination

Heavy metals contamination in nature is the main problem in many countries. The major threats to human health from heavy metals, such as lead, cadmium, copper and mercury, are associated with exposure to them. Consumption of the trace amount of heavy metals in water could cause a detrimental risk to human health. These metals have been widely studied and their effects on human health have been regularly reviewed by international organizations such as the World Health Organization (WHO). Keeping heavy metal concentration under control should be considered in order to propose techniques with suitable limit of detection, according to Guideline. Table 1.1 presents Guideline in drinking water by the World Health Organization (WHO) [29]. Therefore, it is essential to search for a rapid, sensitive, and simple method for detection and monitoring of these contaminants in water.

Table 1.1 Guideline values for chemicals that are of health significance in drinking water.

Chemical	Guideline	Remarks
	$\mu\text{g L}^{-1}$ (ppb)	
Arsenic (As)	10	
Chromium (Cr)	50	For total chromium
Selenium (Se)	40	
Cadmium (Cd)	3	
Mercury (Hg)	6	For inorganic mercury
Lead (Pb)	10	

There are various conventional techniques to analyze heavy metal contaminated in water, for instance, atomic absorption spectrometry [30-32], inductively coupled plasma optical emission spectrometry [33-35], and inductively coupled plasma mass spectrometry [36, 37]. However, these spectrometric instruments still have some drawbacks which are bulky, expensive, low sensitive and not suitable for on-site analysis [38, 39]. To overcome these disadvantages, the electrochemical techniques became an alternative technique to preconcentration heavy metal ions due to high sensitivity, high precision, relatively low cost, and portability [40].

1.4 Introduction of electrochemistry and its applications

The electrochemical techniques provide information on the processes taking place when an electric potential is applied to the system under study. Electrochemistry can be used to investigate the release of electrons (called oxidation) or receiving of electrons (reduction) that experienced by an electrode material during electrical incentive. Redox reaction are

consisted of oxidation and reduction reactions. The information about the reaction mechanisms, concentration, intermediate, dynamic, and other nature of a species in sample solution can be examined in virtue of redox reaction. Generally, there are two kinds of electrochemical cells, which are galvanic cell and electrolytic cell. Galvanic cell produces an electric current from energy released by a spontaneous redox reaction. On the other hand, electrolytic cell requires an external source of electrical energy to induce a chemical reaction. Electrolytic method have many advantages, for instance, high sensitivity with a wide linear dynamic range of concentration for both inorganic and organic species, simplicity, rapid analysis time and simultaneous detection of various target analytes. The selection of the electrochemical techniques depends on the nature of ions or compounds of interest and its interferences in surrounding environment. The following details in this section will focus on the electrochemical techniques that were used in this work.

Voltammetry is an electrochemical technique, which is based on the application of a potential to an electrode surrounded with an electrolyte containing electro-active species and measuring the signal as a current flowing through that electrode. Voltammetric electrochemical cell consists of three electrodes, which are working electrode (WE), counter electrode (CE), and reference electrode (RE). Each electrode have their specific characteristics. Working electrode is the most important electrode of electrochemical cell because the interested reaction will occur at the surface of this electrode. Next, counter electrode or auxiliary electrode is an electrode used in a three-electrode electrochemical cell for voltammetric analysis or other reactions in which an electric current is expected to flow. This electrode will make the potential of reference electrode remain constant since no electron flow through. Lastly, the reference electrode is an electrode with a steady and recognized electrode potential. Using buffered or saturated concentration of interested target species in the redox reaction solution, electrode

potential will be generally accomplished high stability. Occasionally, the potential that applied in the system changed as a function of time was controlled.

In this work, deposition step involves the electrolytic deposition of a small part of the target metal ions in the solution on the working electrode for the preconcentration of analytes. For metal ions deposition, preconcentration step is performed by cathodic deposition (negative potential) as a controlled time and applied potential. The deposition potential is more negative than standard potential (E^0) to completely and easily reduce the metal ions in solution. The metal ions reach the working electrode by diffusion and convection.

1.5 Purpose and outlines

In this plasma of AC-LEP, an air bubble remained in the LEP channel during plasma generation by AC power source. The bubble is expected to affect plasma generation strongly. In order to investigate in detail the effect of the bubbles, we fabricated a microfluidic system to introduce different kinds of gas bubbles intentionally into the LEP channel. After that, optimization of all experimental parameters will be done to improve gas bubble generation. Next, preliminary experiment results revealed that less channel damage was observed when using AC-LEP compared to DC-LEP. However, the effect of gas introduction is still unclear. In this study, we will study the effect of various type of gas by introduction of bubble and detailed comparison with DC-LEP. Finally, this technique can be used as a metal in real sample. To wider the application of AC-LEP, the integration of two techniques for heavy metal detection was studied. A more chemical-specific determination conditions can be achieved by choosing the reasonable applied voltage for the oxidation / reduction potential and working electrode material. Target compounds (analytes) are separated using a specific voltage in

reduction reaction process. After separation, the compounds present at working electrode will be directly desorption and detection by using LEP.

1.6 Dissertation organization

Chapter I presents a general introduction to plasma, some development of discharge plasmas with versatile configurations and their applications to heavy metal ions detection. In this part, many research about LEP also summarized. Besides, detail explanation of heavy metal contamination and electrochemical method that will be combined with LEP. Finally, the objectives of dissertation is pointed out.

Chapter II presents a study of effect of gas bubble to the micro plasma of LEP. The microchip configuration is proposed in order to generate stable and continuous gas bubbles. The effect of flow rate, size of both gas and liquid channel, and type of gas on the plasma is presented. This gas generation part will be integrated to plasma generation to observe the contribution of gas.

Chapter III presents the effect study of gas onto AC-LEP and DC-LEP. The integration of gas bubble generation part to plasma generation zone revealed the contribution of plasma generation of introduced gases in both cases, AC-LEP and DC-LEP. Because low channel damage is found in case of AC-LEP, we assume that the presence of gas and plasma generation process might be different from DC-LEP.

Chapter IV shows a feasibility of integrated techniques, which are electrodeposition and LEP-OES for improvement of heavy metal detection. Some experimental parameters are characterized. Chip design, measurement protocol, data acquisition and processing are proposed to be suitable with the combination of the novel LEP with electrodeposition. This

part is also presenting the application of the novel integrated chip for the quantitative detection of lead.

Chapter V gives some general conclusions and notable points throughout the dissertation.

1.7 References

- [1] Introduction to Theoretical and Applied Plasma Chemistry, in: A. Fridman (Ed.) Plasma Chemistry, Cambridge University Press, Cambridge, 2008, pp. 1-11.
- [2] W.G. Graham, K.R. Stalder, Plasmas in liquids and some of their applications in nanoscience, *Journal of Physics D: Applied Physics*, 44 (2011) 174037.
- [3] P. Jamroz, K. Greda, P. Pohl, Development of direct-current, atmospheric-pressure, glow discharges generated in contact with flowing electrolyte solutions for elemental analysis by optical emission spectrometry, *TrAC Trends in Analytical Chemistry*, 41 (2012) 105-121.
- [4] M.R. Webb, G.M. Hieftje, Spectrochemical analysis by using discharge devices with solution electrodes, *Anal Chem*, 81 (2009) 862-867.
- [5] T. Krahling, A. Michels, S. Geisler, S. Florek, J. Franzke, Investigations into modeling and further estimation of detection limits of the liquid electrode dielectric barrier discharge, *Anal Chem*, 86 (2014) 5822-5828.
- [6] R. Shekhar, D. Karunasagar, M. Ranjit, J. Arunachalam, Determination of elemental constituents in different matrix materials and flow injection studies by the electrolyte cathode glow discharge technique with a new design, *Anal Chem*, 81 (2009) 8157-8166.
- [7] Y. Kanzaki, M. Hirabe, O. Matsumoto, Glow Discharge Electrolysis of Aqueous Sulfuric Acid Solution in Various Atmosphere, *Journal of The Electrochemical Society*, 133 (1986) 2267-2270.

- [8] R.K. Marcus, W.C. Davis, An atmospheric pressure glow discharge optical emission source for the direct sampling of liquid media, *Anal Chem*, 73 (2001) 2903-2910.
- [9] M.R. Webb, F.J. Andrade, G.M. Hieftje, Use of electrolyte cathode glow discharge (ELCAD) for the analysis of complex mixtures, *Journal of Analytical Atomic Spectrometry*, 22 (2007) 766.
- [10] P. Mezei, T. Cserfalvi, Electrolyte Cathode Atmospheric Glow Discharges for Direct Solution Analysis, *Applied Spectroscopy Reviews*, 42 (2007) 573-604.
- [11] T. Cserfalvi, P. Mezei, P. Apai, Emission studies on a glow discharge in atmospheric pressure air using water as a cathode, *Journal of Physics D: Applied Physics*, 26 (1993) 2184-2188.
- [12] J. Yu, X. Zhang, Q. Lu, D. Sun, X. Wang, S. Zhu, Z. Zhang, W. Yang, Evaluation of analytical performance for the simultaneous detection of trace Cu, Co and Ni by using liquid cathode glow discharge-atomic emission spectrometry, *Spectrochimica Acta Part B: Atomic Spectroscopy*, 145 (2018) 64-70.
- [13] M.R. Webb, F.J. Andrade, G. Gamez, R. McCrindle, G.M. Hieftje, Spectroscopic and electrical studies of a solution-cathode glow discharge, *Journal of Analytical Atomic Spectrometry*, 20 (2005) 1218.
- [14] M.R. Webb, F.J. Andrade, G.M. Hieftje, Compact glow discharge for the elemental analysis of aqueous samples, *Anal Chem*, 79 (2007) 7899-7905.
- [15] W. Zu, Y. Yang, Y. Wang, X. Yang, C. Liu, M. Ren, Rapid determination of indium in water samples using a portable solution cathode glow discharge-atomic emission spectrometer, *Microchemical Journal*, 137 (2018) 266-271.
- [16] A.J. Schwartz, K.L. Williams, G.M. Hieftje, J.T. Shelley, Atmospheric-pressure solution-cathode glow discharge: A versatile ion source for atomic and molecular mass spectrometry, *Anal Chim Acta*, 950 (2017) 119-128.

- [17] M. Miclea, K. Kunze, J. Franzke, K. Niemax, Plasmas for lab-on-the-chip applications, *Spectrochimica Acta Part B: Atomic Spectroscopy*, 57 (2002) 1585-1592.
- [18] U. Kogelschatz, Dielectric-Barrier Discharges: Their History, Discharge Physics, and Industrial Applications, *Plasma Chemistry and Plasma Processing*, 23 (2003) 1-46.
- [19] Q. He, Z. Zhu, S. Hu, H. Zheng, L. Jin, Elemental determination of microsamples by liquid film dielectric barrier discharge atomic emission spectrometry, *Anal Chem*, 84 (2012) 4179-4184.
- [20] Y. Zhou, Y. Hong, Z. Li, Z. Bi, J. Zhang, J. Niu, J. Pan, J. Li, Y. Wu, Investigation of discharge characteristics of DBD plasma produced with multi-needle to plate electrodes in water by optical emission spectroscopy, *Vacuum*, 162 (2019) 121-127.
- [21] A. Iiduka, Y. Morita, E. Tamiya, Y. Takamura, Optical Emission Spectrometer of Aqueous Solution Samples Employing Liquid Electrode Plasma, in: J.N. Thomas Laurell, Klavs Jensen, D. Jed Harrison and Jörg P. Kutter (Ed.) 8th International Conference on Miniaturized Systems for Chemistry and Life Sciences, The Royal Society of Chemistry, Malmö, Sweden, 2004, pp. 423.
- [22] A. Kitano, A. Iiduka, T. Yamamoto, Y. Ukita, E. Tamiya, Y. Takamura, Highly sensitive elemental analysis for Cd and Pb by liquid electrode plasma atomic emission spectrometry with quartz glass chip and sample flow, *Anal Chem*, 83 (2011) 9424-9430.
- [23] N.H. Tung, M. Chikae, Y. Ukita, P.H. Viet, Y. Takamura, Sensing technique of silver nanoparticles as labels for immunoassay using liquid electrode plasma atomic emission spectrometry, *Anal Chem*, 84 (2012) 1210-1213.
- [24] D. Van Khoai, A. Kitano, T. Yamamoto, Y. Ukita, Y. Takamura, Development of high sensitive liquid electrode plasma – Atomic emission spectrometry (LEP-AES) integrated with solid phase pre-concentration, *Microelectronic Engineering*, 111 (2013) 343-347.

- [25] M. Banno, E. Tamiya, Y. Takamura, Determination of trace amounts of sodium and lithium in zirconium dioxide (ZrO₂) using liquid electrode plasma optical emission spectrometry, *Anal Chim Acta*, 634 (2009) 153-157.
- [26] D. Van Khoai, T. Yamamoto, Y. Ukita, Y. Takamura, On-chip solid phase extraction–liquid electrode plasma atomic emission spectrometry for detection of trace lead, *Japanese Journal of Applied Physics*, 53 (2014) 05FS01.
- [27] S. Barua, I.M.M. Rahman, M. Miyaguchi, A.S. Mashio, T. Maki, H. Hasegawa, On-site analysis of gold, palladium, or platinum in acidic aqueous matrix using liquid electrode plasma-optical emission spectrometry combined with ion-selective preconcentration, *Sensors and Actuators B: Chemical*, 272 (2018) 91-99.
- [28] K. Do Van, M. Hidekazu, Y. Tamotsu, T. Phan Trong, O. Akitoshi, T. Yuzuru, Development of AC-driven liquid electrode plasma for sensitive detection of metals, *Japanese Journal of Applied Physics*, 55 (2016) 02BC23.
- [29] W.H. Organization, *Guidelines for Drinking-Water Quality: Fourth Edition Incorporating the First Addendum*, Geneva, 2017.
- [30] S. Khazaeli, N. Nezamabadi, M. Rabani, H.A. Panahi, A new functionalized resin and its application in flame atomic absorption spectrophotometric determination of trace amounts of heavy metal ions after solid phase extraction in water samples, *Microchemical Journal*, 106 (2013) 147-153.
- [31] M.A. Alvarez, G. Carrillo, Simultaneous determination of arsenic, cadmium, copper, chromium, nickel, lead and thallium in total digested sediment samples and available fractions by electrothermal atomization atomic absorption spectroscopy (ET AAS), *Talanta*, 97 (2012) 505-512.

- [32] M.T. Naseri, M.R. Hosseini, Y. Assadi, A. Kiani, Rapid determination of lead in water samples by dispersive liquid-liquid microextraction coupled with electrothermal atomic absorption spectrometry, *Talanta*, 75 (2008) 56-62.
- [33] C. Cui, M. He, B. Chen, B. Hu, Restricted accessed material-copper(II) ion imprinted polymer solid phase extraction combined with inductively coupled plasma-optical emission spectrometry for the determination of free Cu(II) in urine and serum samples, *Talanta*, 116 (2013) 1040-1046.
- [34] A. Beiraghi, S. Babae, M. Roshdi, Simultaneous preconcentration of cadmium, cobalt and nickel in water samples by cationic micellar precipitation and their determination by inductively coupled plasma-optical emission spectrometry, *Microchemical Journal*, 100 (2012) 66-71.
- [35] L. Zhao, S. Zhong, K. Fang, Z. Qian, J. Chen, Determination of cadmium(II), cobalt(II), nickel(II), lead(II), zinc(II), and copper(II) in water samples using dual-cloud point extraction and inductively coupled plasma emission spectrometry, *J Hazard Mater*, 239-240 (2012) 206-212.
- [36] C.Y. Tai, S.J. Jiang, A.C. Sahayam, Determination of As, Hg and Pb in herbs using slurry sampling flow injection chemical vapor generation inductively coupled plasma mass spectrometry, *Food Chem*, 192 (2016) 274-279.
- [37] R.P. Lamsal, D. Beauchemin, Estimation of the bio-accessible fraction of Cr, As, Cd and Pb in locally available bread using on-line continuous leaching method coupled to inductively coupled plasma mass spectrometry, *Anal Chim Acta*, 867 (2015) 9-17.
- [38] Y. Wei, C. Gao, F.L. Meng, H.H. Li, L. Wang, J.H. Liu, X.J. Huang, SnO₂/Reduced Graphene Oxide Nanocomposite for the Simultaneous Electrochemical Detection of Cadmium(II), Lead(II), Copper(II), and Mercury(II): An Interesting Favorable Mutual Interference, *J Phys Chem C*, 116 (2012) 1034-1041.

- [39] C. Gao, X.Y. Yu, R.X. Xu, J.H. Liu, X.J. Huang, AlOOH-reduced graphene oxide nanocomposites: one-pot hydrothermal synthesis and their enhanced electrochemical activity for heavy metal ions, *ACS Appl Mater Interfaces*, 4 (2012) 4672-4682.
- [40] U. Injang, P. Noyrod, W. Siangproh, W. Dungchai, S. Motomizu, O. Chailapakul, Determination of trace heavy metals in herbs by sequential injection analysis-anodic stripping voltammetry using screen-printed carbon nanotubes electrodes, *Anal Chim Acta*, 668 (2010) 54-60.

CHAPTER II

DEVELOPMENT OF THE LIQUID ELECTRODE PLASMA (LEP) CHIP WITH GAS INTRODUCTION

2.1 Introduction

The main purpose of this study is to investigate the mechanism of low channel damage of alternating current liquid electrode plasma (AC-LEP). From previous work, direct current liquid electrode plasma (DC-LEP) was used as excitation source for elemental analysis. However, severe channel damage was found after using for short time [1]. After that, we found the better conditions to generate LEP by alternating current with higher stability and significantly low damages on micro channel, called the new method as AC-LEP [2]. The videos recorded by a high-speed camera showed that gas bubbles remained in the liquid micro channel during plasma generation by the AC power source. Under the applied voltage, the bubbles expand and plasma appeared inside the bubbles, after which the bubbles began to shrink. Hence, a suitable flow was required to maintain bubbles inside the narrow channel, which was a clearly different mechanism than in DC-LEP. In order to understand the effect of bubble in AC-LEP system, new chip was designed to continuously introduce into LEP system.

The new chip design was adapted from droplet-based microfluidic systems. Droplets of one fluid in a second immiscible fluid are useful in a wide range of applications. Moreover, miniature gas sensor devices for gas compositions determination have attracted increasing interest due and use the similar channel configuration [3]. In order to understand the effect of bubble to the plasma generation, stable and controllable bubble generation from outside microchannel was required. A promising approach is to use microfluidic systems, which

consist of networks of channels of normally 10–100 μm diameter [4]. For controllable applications of microbubbles, their generation mechanisms indifferent micro-fluidic devices are very necessary. Many relevant studies have been reported in literatures involving the T-junction [5], Y-junction [6], cross-junction [7], flow-focusing [8] and some other kinds of microfluidic devices [9, 10], as shown in Fig. 2.1.

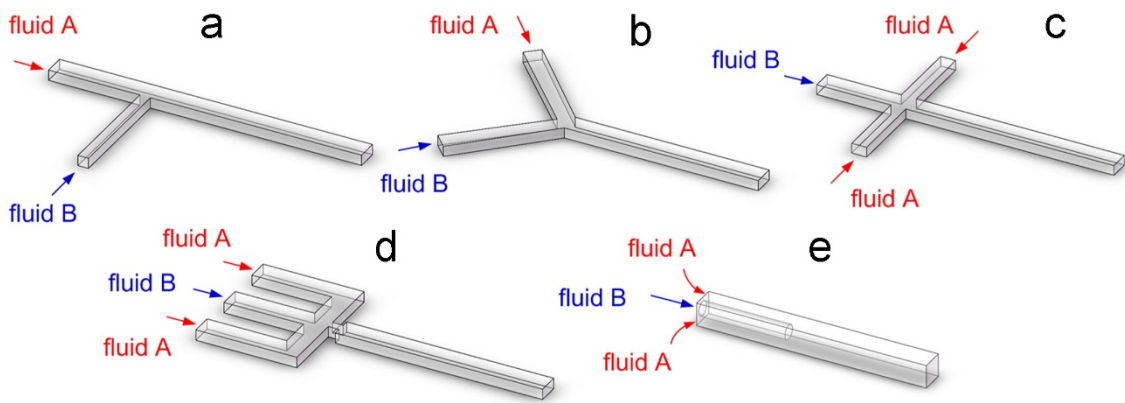


Figure 2.1 Some common microfluidic devices used for microbubble and micro droplet generations. (a) T-junction microchannel; (b) Y-junction microchannel; (c) cross-junction microchannel; (d) flow focusing microfluidic device; (e) co-flowing microfluidic device. [11]

From many designs of bubble generation system, flow focusing microfluidic device was selected because of simplicity and ease of parameters adjustment. In addition, flow focusing microfluidic device was combined with bubble-based gas sensing [3]. The bubble-based gas sensor comprises gas and liquid channels along with a nozzle to produce gas bubbles through a micro-structure. The results showed the stable bubble generation and was simple in structure and fabrication.

In this part of study, the gas flow channel introduces the gas stream between the two liquid flows that are provided by the liquid flow channels. The two immiscible phases flow down the inlet channels (one central channel for gas, and the two outer channels for liquid) and meet at the junction of these channels upstream of the transition position before entering to next part of the chip. The chip dimension was fabricated in different length and width to evaluate the stability of bubble generation. Moreover, this bubble generation part will connect to LEP to observe the effect of bubble to plasma stability and signal intensity.

2.2 Fabrication of new microchip design including gas channel

All reagents used in this study were analytical reagent grade and were used without further purification. The PDMS layer is attached onto a glass slide that is a substrate for the chip. The channel is carved on the PDMS sheet by a photolithographic technique. There are two inlets, liquid inlet and gas inlet, and one outlet on the chip. The width of the channel is 50 μm and the depth of the channel on PDMS sheet is around 100 μm and is determined by the height of photoresist patterned on silicon wafer. Two 2-mm diameter holes were punched at each end of the LEP channel. Finally, the PDMS layer and the substrate are bound together by oxygen plasma. Both liquid and gas were pushed by syringe pump with same speed and then observed with microscope in Fig. 2.2. Types of selected gases in this work are Ar gas, nitrogen gas, oxygen gas and air.

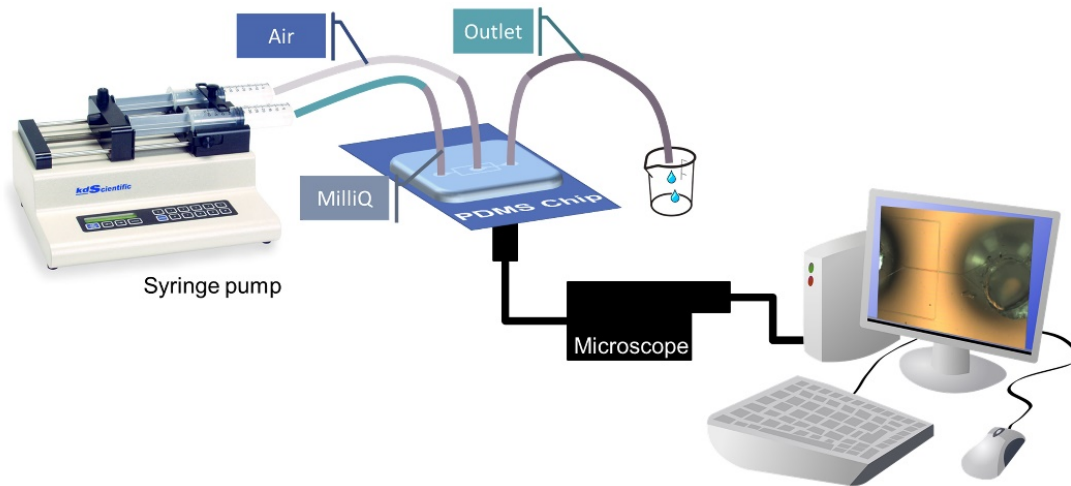


Figure 2.2 Experimental setup

Pattern design for microchip

The film mask was design with computer software (Adobe Illustrator) according to the previous publications that observe bubble generation in various phase, for example, water-in-oil droplet and gas-in-oil droplet. Fig. 2.3 is illustrated the design of microchip pattern. The dimension of this pattern are inlet and outlet diameter is 2 mm, width of channel is varied from 50, 100, and 150 μm , and overall size is 0.5×2 cm. After that, bubble generation part was integrated to plasma generation region to further investigate the effect of presence of bubble before, during and after plasma generation.

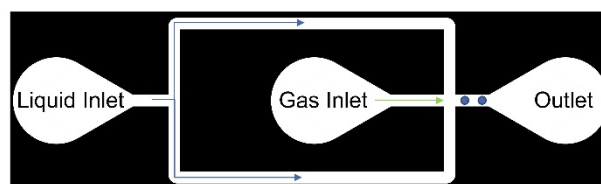


Figure 2.3 Film Mask Pattern

Fabrication of PDMS mold and chip

The PDMS layer was made by molding and lithographic methods. The fabrication process is shown in Fig. 2.4. First, a silicon wafer was sequentially cleaned with acetone, ethanol, and then deionized (DI) water. Permanent epoxy negative photoresist SU-8 3050 was poured on a silicon wafer and spin coated at 1000 rpm for 30 s, then soft baked on a hotplate at 95°C for 45 min, exposed to UV light for 30 s, and finally post-baked on a hot plate at 65°C for 1 min and then 95°C for 5 min. The silicon wafer was then cooled to room temperature and the channel pattern was developed with SU-8 developer, followed by rinsing with isopropanol. A PDMS monomer mixed with 10 wt. % curing catalyst was poured onto the fabricated mold and cured at 75°C for 90 min. The PDMS replica layer was peeled off and punched to make 2-mm-diameter holes for the inlet and outlet. The obtained PDMS layer was bonded with the glass substrate by oxygen plasma bonding (75 W for 10 s). Finally, the as-fabricated chip was connected to tubes and connected to two platinum electrodes (0.3 mm diameter, 5 cm length). The final microchip configuration was shown in Fig 2.5.

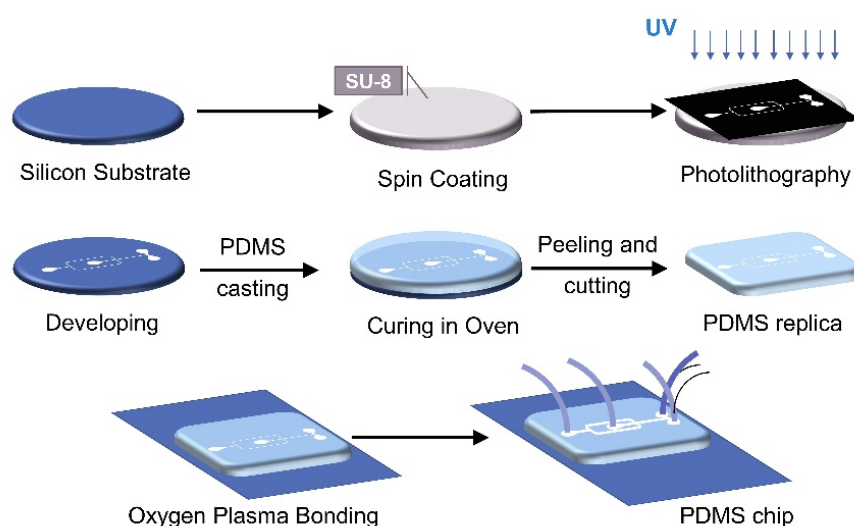


Figure 2.4 Schematic flow of chip fabrication. Negative photolithography was utilized for mold fabrication. After putting silicone tubes, all connection points were sealed by PDMS to prevent leakage.

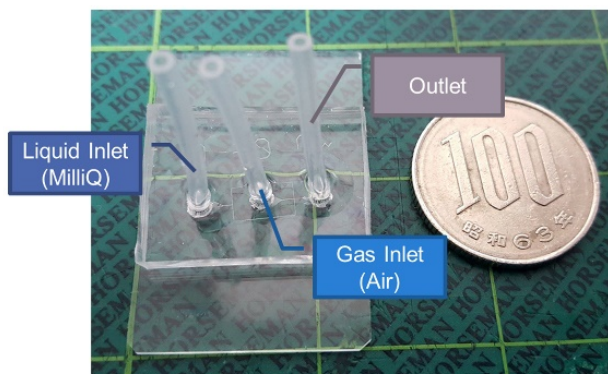


Figure 2.5 Ready-to-use PDMS chip

Next, Fig. 2.6 illustrated that the microchips were investigated under microscope and shown well fabricated channel which was ready for the next step of experiment. The channel dimension was same as the dimension of mold.

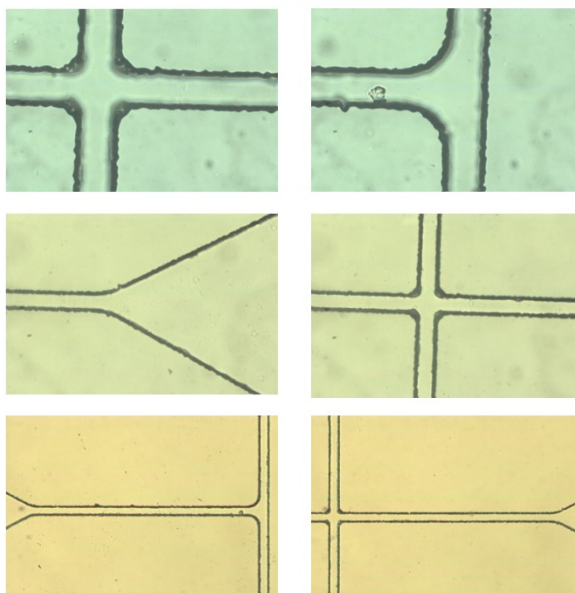


Figure 2.6 Shape of finished PDMS chip under microscope

Observation of bubble generation process

After that, all channels were filled with Milli Q and gas to observe bubbles with the speed of $30 \mu\text{L min}^{-1}$ as of optimized flow rate in plasma generation process. The pictures and videos from microscope confirmed that by using this system, we could generate bubbles, as shown in Fig. 2.7. The bubble was formed after passing through the intersection which was matched with previous studied. However, many experimental parameters need to optimize to obtain the stable and reproducible bubble generation.

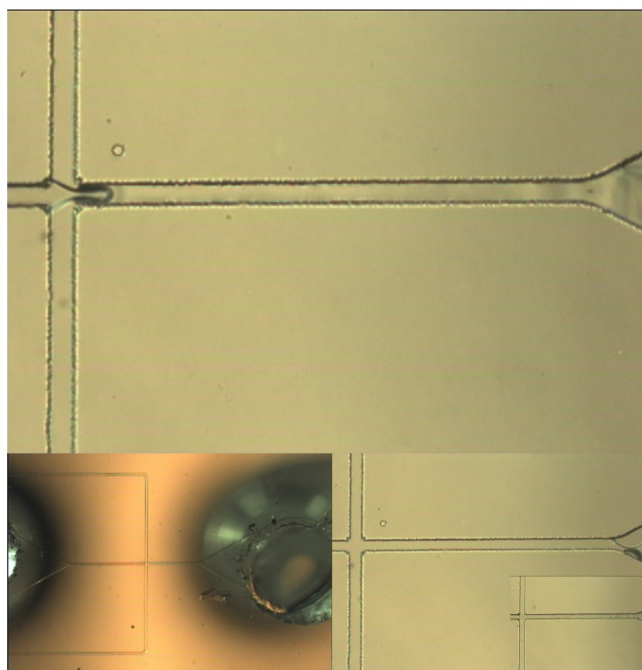


Figure 2.7 Picture of generated bubbles inside channel

2.3 Optimization of experimental parameters

2.3.1 Liquid and gas channel size

The results of different size of channel were summarized in Fig.2.8, which divided into three groups, liquid channel size is bigger than gas channel size (in left column), liquid channel size is the same size as gas channel size (in the center column), and liquid channel size is smaller than gas channel size (in the right column). Most of the chips showed a stable bubble generation especially 50–50 μm and 50–100 μm that had a very stable, not too large bubble size and not too slow generation. For smaller gas channel size, the gas was hard to divide into small bubbles. On the other hand, when gas channel size was bigger, it became quite hard to push out the gas especially with small liquid channel size. Because of the pressure of gas and liquid inside of channel was different, the flow rate of gas and liquid must be optimized to achieve the suitable pressure condition for reproducible bubble generation.




Liquid channel > Gas channel	Liquid channel = Gas channel	Liq. channel < Gas channel
100 – 50 μm	★ 50 – 50 μm	★ 50 – 100 μm
150 – 50 μm	100 – 100 μm	50 – 150 μm
150 – 100 μm	150 – 150 μm	100 – 150 μm
- Very big bubbles - Connected bubble	- Slow generation - Very big bubbles	- Slow generation - Very big bubbles
	- Except for 50-50 μm	

Figure 2.8 . Summary of different channel size of bubble generation

2.3.2 Gas flow rate

The investigation of the bubble generation with different size of channel revealed that the size of bubble depended on flow rate and size of channel. Then, the different flow rate of

gas was studied. In this part, 100-50 μm , 50-50 μm and 50-100 μm chips were selected because they all gave the most stable bubble generation and not big bubble size. The flow rate of gas were set at 10 $\mu\text{L min}^{-1}$, 30 $\mu\text{L min}^{-1}$, 50 $\mu\text{L min}^{-1}$, and 100 $\mu\text{L min}^{-1}$, respectively. On the other hand, the solution flow rate was fixed at 30 $\mu\text{L min}^{-1}$ as an optimized value of solution flow rate. The results showed that too high gas flow rate was not suitable for bubble generation; however, most of the chip could generate stable bubble with different speed and size, as concluded in Fig.2.9.

Gas Flow Rate	Liquid channel > Gas channel 100 – 50 μm	Liquid channel = Gas channel 50 – 50 μm	Liquid channel < Gas channel 50 – 100 μm
10 $\mu\text{L min}^{-1}$	slow	small + slow	 N/A
30 $\mu\text{L min}^{-1}$ (Same flow rate with solution)	 not stable	stable	stable generation
50 $\mu\text{L min}^{-1}$	slow + quite stable	big bubbles	stable generation
100 $\mu\text{L min}^{-1}$	 big + not quite stable	big + not quite stable	big + ~ stable

N/A: No bubble generated

Figure 2.9 Summary of different channel size of bubble generation and different gas flow rate.

Then, nitrogen gas was introduced to this generation system for investigation of bubble behavior. The 50-50 μm and 50-100 μm chips were selected because they all gave the most stable and bubble generation and not big bubble size. Besides, the flow rate of gas were set at 10 $\mu\text{L min}^{-1}$, 30 $\mu\text{L min}^{-1}$, and 50 $\mu\text{L min}^{-1}$. The results illustrated that there were no obvious different between air and nitrogen gas during bubble generation process. However, for the plasma generation, there must be different between air and nitrogen gas due to different

composition and different energy for generate plasma. In Fig.2.10 is a summary of nitrogen gas generation.

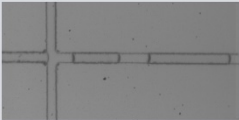
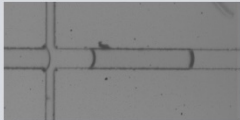
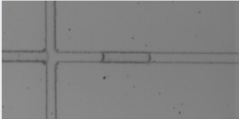
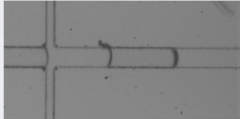
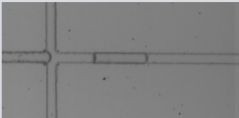
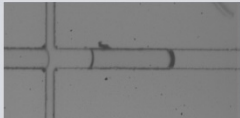
Gas Flow Rate	Liquid channel = Gas channel 50 – 50 μm	Liquid channel < Gas channel 50 – 100 μm
10 $\mu\text{L min}^{-1}$		
30 $\mu\text{L min}^{-1}$ (Same flow rate with solution)		
50 $\mu\text{L min}^{-1}$		

Figure 2.10 Photos of generated bubbles inside channel

The photos from camera in Fig. 2.11 confirmed that by using this system, we could generate bubble. It can be seen that the size of bubble was varied because of very high flow rate of gas; therefore, it was very difficult to control the size and position. To get more precise controlled size and position of bubble, gas flow rate must be lower. The slowest flow rate of gas can be set at 0.03 $\mu\text{L min}^{-1}$ as the lowest speed value of syringe pump. With lower gas flow rate, number of bubble was significantly reduced which might better than of interruption by many bubbles. After that, the bubble generation system was combined to plasma generation system on the same chip. For argon gas bubble, there was no obvious different behavior of gas compare to nitrogen gas or air. Next, with continuous flow of gas bubble in liquid, plasma was generated. Plasma was quite stable inside the center part of channel and the damage was slowly graduated observed. However, severe damage to channel was detected when there was absent of either solution or gas. Thus, optimization of both gas and liquid flow is necessary in order

to get the improved channel damage. In addition, even the size of channel before expected plasma generation zone was smaller, plasma still generated at the desired position.

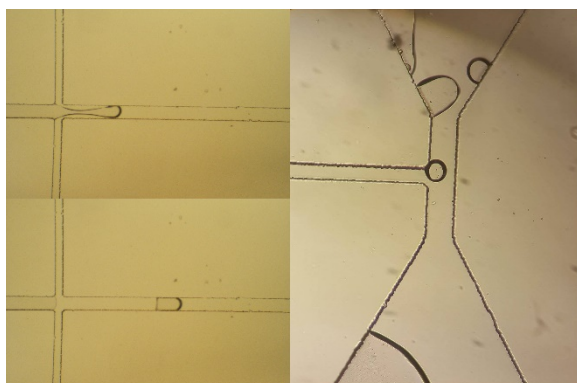


Figure 2.11 Generated Bubbles inside channel

2.3.3 Types of gases

To compare the effect of type of introduced gas, Ar gas, nitrogen gas, oxygen gas, and air were selected. Oxygen gas was selected because it is a product of hydrolysis of water at Pt electrode [2] but we would not use hydrogen gas due to safety procedure. Nitrogen gas was representative of inert and diatomic molecule and might found from vaporization of nitric acid, which is used as solvent in this system. Air was selected due to the abundance of availability in environment and ease of use. Lastly, Ar gas was an inert gas that normally use in ICP system as an carrier gas therefore it might facilitate the plasma generation. Moreover, Ar gas is a monoatomic molecule which is easy to ionize and transfer excess energy to other species in the surrounding area. In order to investigate the effect of gas bubble upon plasma generation, the integrated system was implemented to detect 20 ppm and 50 ppm Pb in 0.1 M HNO₃. The generated plasma was shown in Fig 2.12(A) and (B). This light will be transferred through fiber optics and spectrum was achieved in Fig 2.12(C). Two of left and right based line were selected

to draw based line of desired peak of Pb, which is at 405.78 nm. The peak area is corresponding to amount of Pb in sample solution, therefore higher peak area will be represented higher Pb ions in sample solution.

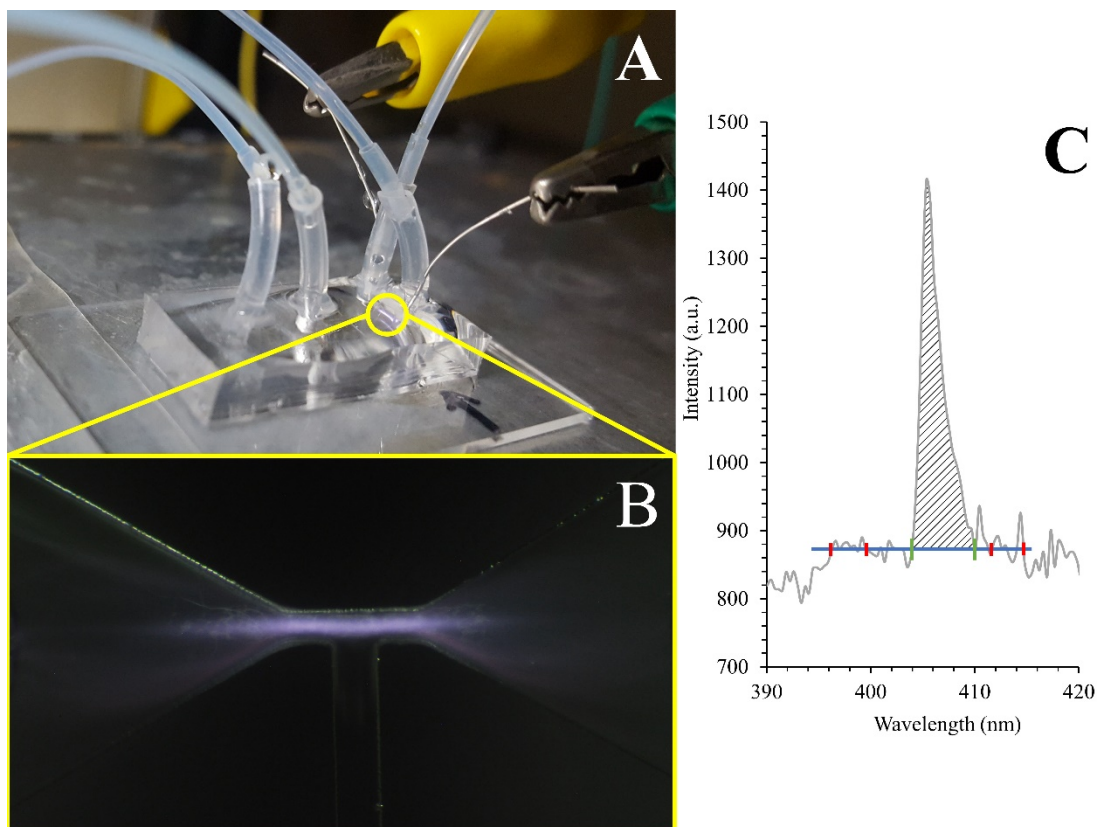


Figure 2.12 Photos of experimental setup with plasma and bubble generation system (A) and plasma inside narrow channel (B). The peak area is calculated by software at desired peak location (C).

The result was shown in Fig. 2.13. The peak area is directly proportional to analyte concentration. At the same analyte concentration, Air introduction system shown the relatively high peak area with low standard deviation (small error bar). While, without gas introduction (original system) shown lower peak area with relatively satisfy standard deviation. This is one of benefits of AC–LEP usually provide stable and reproducible signal intensity.

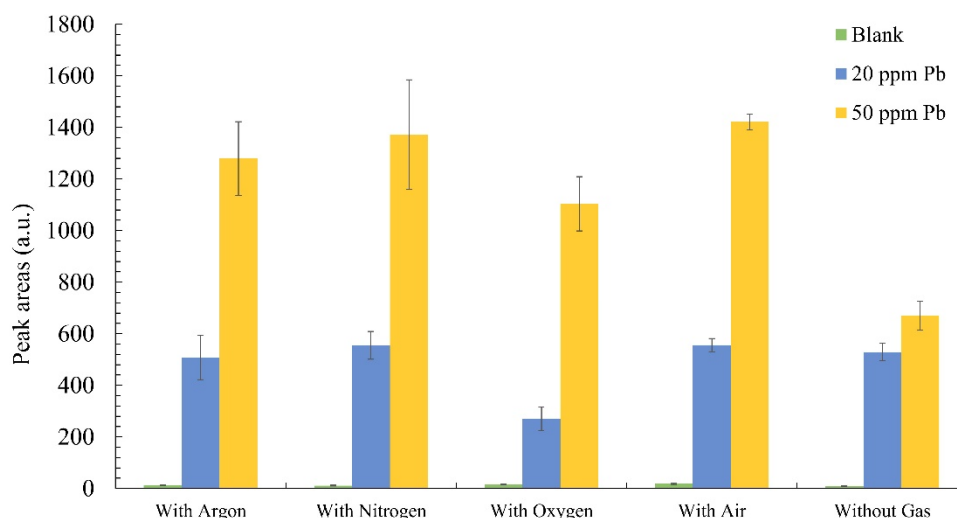


Figure 2.13 Comparison of peak area of different gas introduction system of Pb solution

Time required for plasma generation in case of without gas took around more than 15 seconds, on the other hand, with gas introduction case took less than 3 seconds. We could conclude that without gas introduction, inside narrow was required some time to wait for generated bubble came from electrode and then plasma would generate inside of that bubble. In the contrary, when gas bubble was introduced to the narrow channel externally, plasma took less time to generate inside of presence bubble. From these results, we can confirm that this bubble generation system was successfully facilitate plasma generation and revealed lower channel damage. Moreover, these results suggested that the mechanism of plasma generation in AC-LEP might different from previous DC-LEP. Then, plasma was generated continuously for one hour and photos were taken by time pass. Argon gas system showed the longest chip using lifetime. Finally, the 50 ppm lead concentration were also detected for one hour, as shown in Fig 2.14.

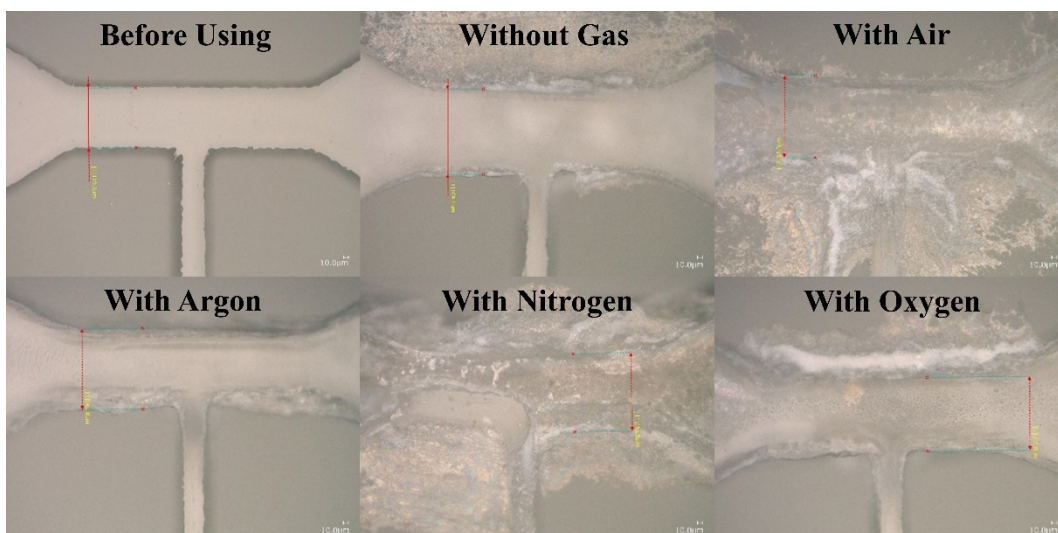


Figure 2.14 Photos of chip before and after used continuously for 1 hour

2.4 Conclusion

In this chapter, the gas bubble generation was successfully fabricated. The optimized conditions of microchip dimension is 50–50 μm of liquid and gas channel. Moreover, the flow rate is also important factor that was 30 μL min⁻¹ of liquid flow rate and 0.03 μL min⁻¹ of gas flow rate. Then, this bubble generation platform was integrated with plasma generation zone. On the new integrated microchip, plasma can be generated with different kinds of gas at different initial time because of different properties of gases. With gas introduction shown that gas bubble was needed to reduce channel damage and should be further study the mechanism of AC–LEP.

2.5 References

- [1] A. Kitano, A. Iiduka, T. Yamamoto, Y. Ukita, E. Tamiya, Y. Takamura, Highly sensitive elemental analysis for Cd and Pb by liquid electrode plasma atomic emission spectrometry with quartz glass chip and sample flow, *Anal Chem*, 83 (2011) 9424-9430.
- [2] D. Van Khoai, H. Miyahara, T. Yamamoto, P.T. Tue, A. Okino, Y. Takamura, Development of AC-driven liquid electrode plasma for sensitive detection of metals, *Japanese Journal of Applied Physics*, 55 (2016) 02BC23.
- [3] A. Bulbul, H. Kim, A bubble-based microfluidic gas sensor for gas chromatographs, *Lab Chip*, 15 (2015) 94-104.
- [4] Y.H. Lin, G.B. Lee, C.W. Li, G.R. Huang, S.H. Chen, Flow-through sampling for electrophoresis-based microfluidic chips using hydrodynamic pumping, *Journal of Chromatography A*, 937 (2001) 115-125.
- [5] J. Tan, S.W. Li, K. Wang, G.S. Luo, Gas-liquid flow in T-junction microfluidic devices with a new perpendicular rupturing flow route, *Chemical Engineering Journal*, 146 (2009) 428-433.
- [6] R. Pohorecki, K. Kula, A simple mechanism of bubble and slug formation in Taylor flow in microchannels, *Chemical Engineering Research & Design*, 86 (2008) 997-1001.
- [7] T. Fu, Y. Ma, D. Funfschilling, H.Z. Li, Gas-liquid flow stability and bubble formation in non-Newtonian fluids in microfluidic flow-focusing devices, *Microfluidics and Nanofluidics*, 10 (2010) 1135-1140.
- [8] M. Hashimoto, S.S. Shevkoplyas, B. Zasonska, T. Szyzborski, P. Garstecki, G.M. Whitesides, Formation of bubbles and droplets in parallel, coupled flow-focusing geometries, *Small*, 4 (2008) 1795-1805.
- [9] M. Hashimoto, G.M. Whitesides, Formation of bubbles in a multisection flow-focusing junction, *Small*, 6 (2010) 1051-1059.

- [10] E. Castro-Hernandez, W. van Hoeve, D. Lohse, J.M. Gordillo, Microbubble generation in a co-flow device operated in a new regime, *Lab Chip*, 11 (2011) 2023-2029.
- [11] K. Wang, L.S. Xie, Y.C. Lu, G.S. Luo, Generating microbubbles in a co-flowing microfluidic device, *Chemical Engineering Science*, 100 (2013) 486-495.

CHAPTER III

STUDY ON EFFECT OF INTRODUCED GAS BUBBLES FOR THE LOW CHANNEL DAMAGE IN DIRECT AND ALTERNATING CURRENT LIQUID ELECTRODE PLASMA ATOMIC EMISSION SPECTROMETRY

3.1 Introduction

Heavy metals are found naturally in the Earth's crust, and become concentrated because of human activities. In developing countries with high population density and insufficient funds available for environmental restoration, low-cost and ecologically sustainable remedial options are required to monitor environment contamination in order to reduce associated health risks and make land available for agricultural production (to improve food security). Recently, many research groups have been developed to investigate miniaturized atmospheric pressure glow discharges (APGD) [1-4], dielectric barrier discharge (DBD) [5, 6], atmospheric pressure liquid discharge [7, 8], liquid electrode plasma (LEP) [9-11] as excitation sources for optical emission spectrometry (OES) of dissolved analytes in liquids for analytical chemistry purposes. The standard methods for elemental analysis, such as inductively coupled plasma (ICP) optical emission spectrometry (OES), atomic absorption spectrometry (AAS), and ICP mass spectrometry (ICP MS) are effective for chemical analysis of aqueous samples and are widely used for routine monitoring of personal exposure because of their high sensitivity, accuracy, and precision. However, these methods require large sample volume and are labor and time intensive. Low-cost, portable, real-time instruments for elemental analysis are needed to avoid these limitations.

Liquid electrode plasma atomic emission spectrometry (LEP-AES) was first introduced by Iiduka *et al.* in 2004.[12] This emission spectrometry method uses microplasma as an excitation source and is suitable for various applications.[13-17] Moreover, the use of LEP-AES in protein sensing studies employing Ag nanoparticle labeling was performed. The proposed technique has various promising applications in metal-nanoparticle-labeled biomolecule detection.[11] This novel technique allows the plasma source to be miniaturized, as no plasma gas or high-power source is required, resulting in compact and portable systems. The device is inexpensive compared with the standard technologies mentioned above and requires minimal training to operate. The channel of microchip is made narrower in between its two ends and contains electrolyte solution. When a voltage pulse is applied to two electrodes at both ends of the micro channel, concentrated electric current generates Joules heating and then water vapor bubble is formed. Inside of generated bubble, micro plasma is appeared from the electrical discharge. Elements in sample solution enter the plasma and emit their specific spectra that are recorded by spectrometer. The principle of LEP is presented in Figure 3.1. LEP is as sensitive as conventional AES methods and requires no plasma gas, low power source, and very small sample usage. Thus, it is useful not only for elemental analysis but also for other high sensitive applications by using specific element as a label [11].

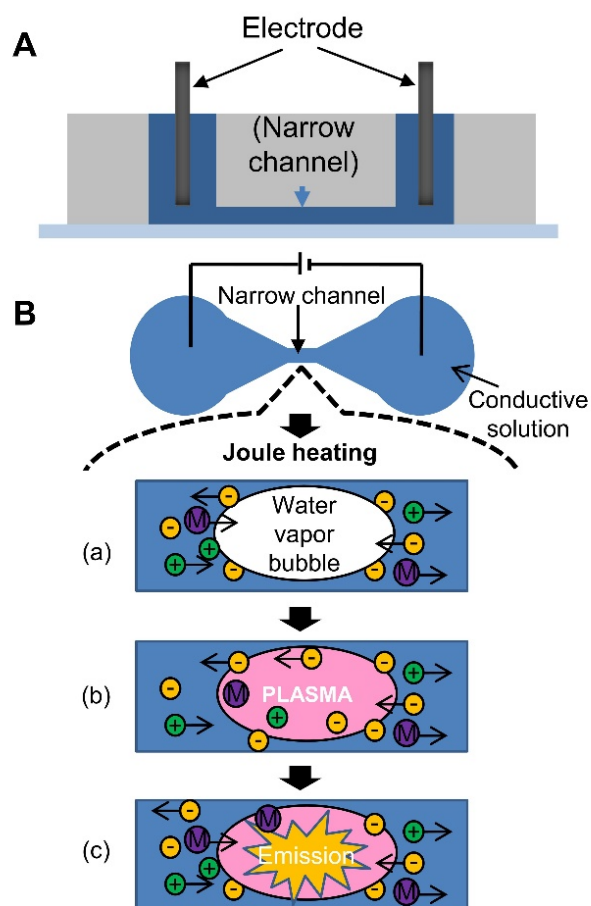


Figure 3.1 Mechanism of liquid electrode plasma optical emission spectrometry. A: Side view of a LEP chip. B: Plan view of LEP channel and mechanism of plasma generation and optical emission. (a) A water vapor bubble generates because of Joule heating when a voltage is applied. (b) Liquid electrode plasma appears in the bubble. (c) Elements in solution enter the plasma and emit their characteristic optical emission lines for quantitative analysis.

In previous studies, LEP systems were developed that were driven by a direct current (DC) source; after repeated measurements, the narrow channel at the center of microchip was clearly deformed due to plasma damage, resulting in a channel width around 1.5 times larger than that in a new microchip [13]. In LEP, high sensitivity and high accuracy are achieved by number of accumulation so that there is a tradeoff between sensitivity/accuracy and lifetime

[13]. Currently, such channel damage limits not only chip lifetime but also sensitivity and accuracy for repeated measurements.

Recently, we demonstrated generation of LEP using alternating current (AC) in a new method called AC-LEP, which showed higher stability and significantly lower microchannel damage (1/3000) than DC-LEP [18]. The plasma was continuously generated in a poly(dimethylsiloxane) (PDMS) chip for about 10 min without severe channel damage or expansion. These observations indicated that AC-LEP showed great potential for reducing channel damage, although the mechanism of this improvement was not clear. In conventional LEP, the plasma gas is generated from the sample solution itself by evaporation due to Joule heating at narrow channel. So, no external gas is required which is the one of the most merits of LEP. In AC-LEP, however, we observed amount of accumulated gas bubbles at both electrodes. High-frequency AC electrolysis of water can occur if the current density is sufficiently high. Thus, it is considerable that the 20 kHz AC signal caused the electrolysis of water, forming a gas product at the two electrodes. In AC-LEP, the accumulated bubbles at the electrode in upper stream flow into LEP and may affect the plasma generation. Therefore, in this study, various types of gases were introduced intentionally from outside into the AC- and DC- LEP and their effects on plasma generation and channel damage were investigated. For that purpose, a new chip design for the introducing gas into the channel was developed. Channel damage was compared in both DC-LEP and AC-LEP with and without gas introduction.

3.2 Optimization of experimental condition for fair comparison of channel expansion

The substrate of the chip was a glass slide, which was coated with a PDMS layer containing a microchannel. The pattern of the LEP chip set up for gas introduction consisted of two liquid inlets, one gas inlet, and one outlet. The plasma generation zone on the LEP chip was 100 μm in both depth and width at the narrowest part of the channel. In the case of the chip without gas introduction, the design described in our previous study was used. The fabrication process is explained in previous chapter.

For LEP determination, the chip was fixed in the experimental setup shown in Fig. 3.2. Both platinum electrodes were connected to either a DC or AC power source. Syringe pumps were used to introduce sample solutions and gas. AC-LEP was generated using a specially designed power-controllable AC power source (maximum voltage of 3 kV, frequency of 20 kHz, Plasma Concept Tokyo Inc., Japan). A DC power supply (Nissei-Giken, Japan) was used for DC-LEP. The plasma was observed with an optical microscope and a UV-VIS spectrophotometer (USB2000, Ocean Optics, USA). The chip dimension was observed using a digital microscope (Keyence VHX-900F and high-magnification zoom lens VH-Z450). For fair comparison of channel damage, both AC-LEP and DC-LEP conditions were optimized to give the same signal intensity (limit of detection, LOD) for Pb in 0.1 M nitric acid. For AC-LEP, a liquid flow rate of 30 $\mu\text{L min}^{-1}$ and Ar gas flow rate of 0.03 $\mu\text{L min}^{-1}$ come together with carrier liquid flow rate of 30 $\mu\text{L min}^{-1}$ (in case of gas introduction) were used. Meanwhile, for DC-LEP, a liquid flow rate of 100 $\mu\text{L min}^{-1}$ was introduced and 1400 V of applied voltage with 3 ms on-time and 2 ms off-time were applied. Emission spectra were acquired using the USB2000 spectrometer (Ocean Optics, USA) and the obtained spectra were analyzed with software (IGOR Pro version 6.3.7.2, WaveMetrics) to calculate the corresponding peak areas. To obtain same LOD in all cases, the optimized conditions were used, and channel damage was

evaluated as a function of plasma duration. Microscopy images were obtained from after first applied voltage for 10 measurements (interval time of 10 s) and then the channel width was measured and compared.

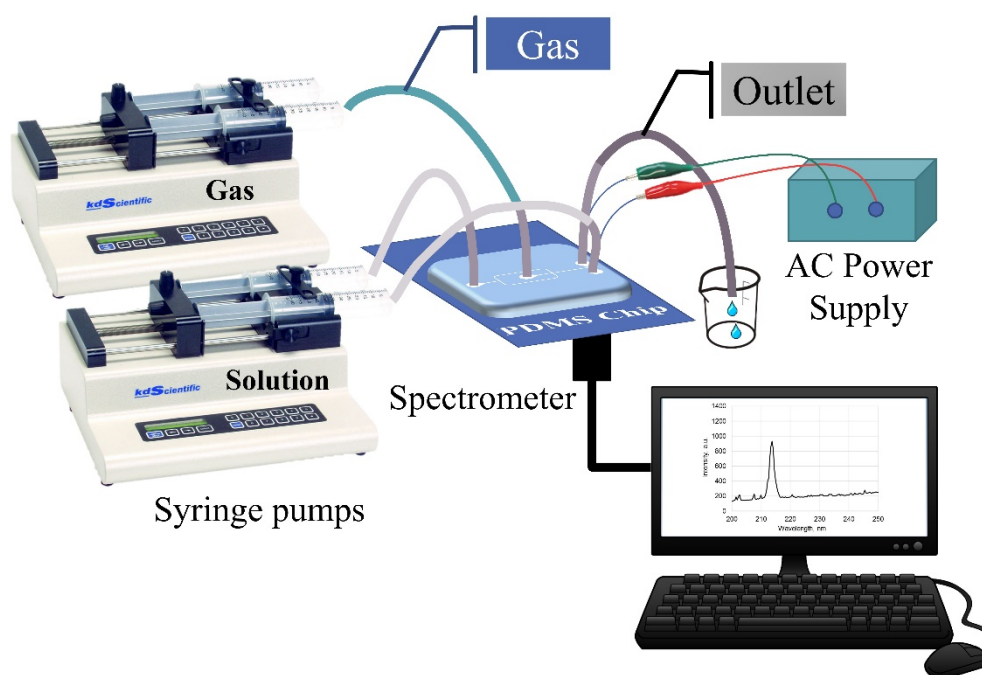


Figure 3.2 Experimental setup

In order to ensure the fair comparison, all of parameters of AC-LEP and DC-LEP were optimized. We confirmed that same signal intensity level (same LOD) is obtained in all cases, as shown in Figure 3.3. Signal intensity can be further improved by increasing applied voltage, however, DC-LEP with high voltage showed huge damage to microchip. Therefore, suitable and reproducible signal intensity should be considered and optimized.

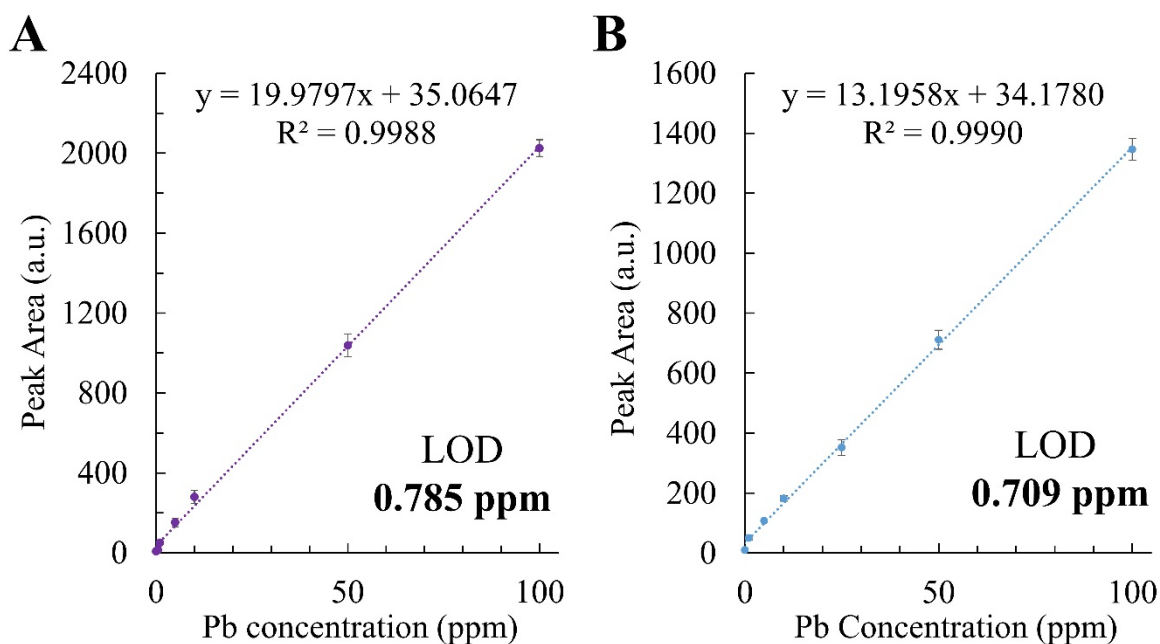


Figure 3.3 Calibration curve of 0 – 100 ppm of lead in 0.1 M nitric acid at optimized conditions from (A) DC-LEP and (B) AC-LEP.

3.3 Channel damage comparison

Channel damage during LEP is the main factor limiting the physical lifetime of PDMS-based chips and measurement reliability, because it decreases the reproducibility of emission signals. We showed in our previous study that the novel AC-LEP significantly reduced channel damage. The microscopy images of a channel before and after AC-LEP (Fig. 3.4A) showed less channel damage compared to the DC-LEP sample (Fig. 3.4B). The channel width increased over the duration of chip usage, resulting in a decrease in the signal intensity due to the higher channel volume. Moreover, remaining bubbles were observed in AC-LEP only, which could be related to the minimal channel damage; therefore, further investigation of these gas bubbles was undertaken.

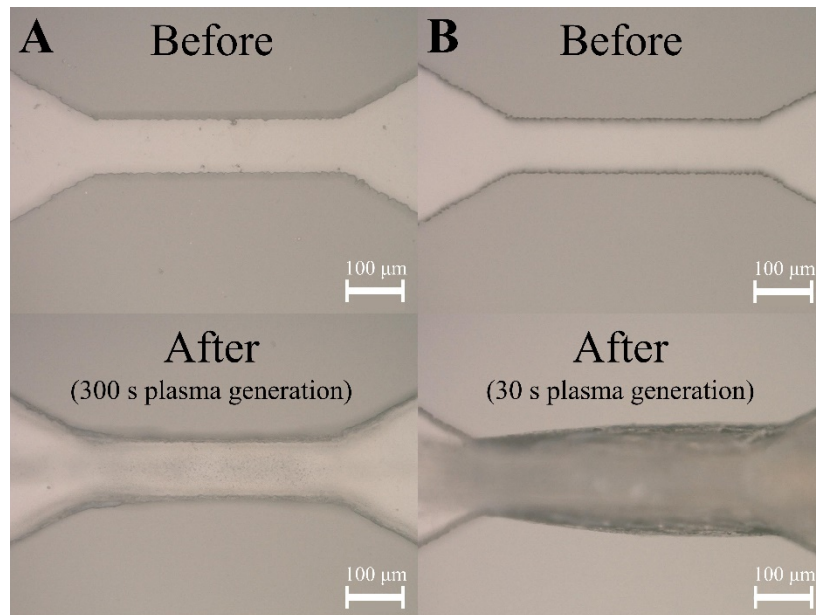


Figure 3.4 Optical microscopy images of channel destruction. LEP channels before and after (A) 300 s of AC-LEP, and (B) 30 s of DC-LEP generation with a voltage of 1400 V.

From the observation of a seed bubble (a very small bubble that nucleates larger bubbles) inside of a narrow channel, chips with a new design were fabricated to allow bubbles generated outside the channel to be introduced into the channel. One of the advantages of LEP is that no plasma gas is required. Hence, in this part of the study, gas was intentionally introduced only to study the mechanism of channel damage, as shown in Figure 3.5. The gas flow rate was optimized to facilitate plasma generation; high flow rates were avoided to prevent the introduced bubbles from disturbing plasma generation. Air and argon gases were selected because argon is often used as a carrier gas to facilitate plasma generation, while air is the easiest gas to use and store.

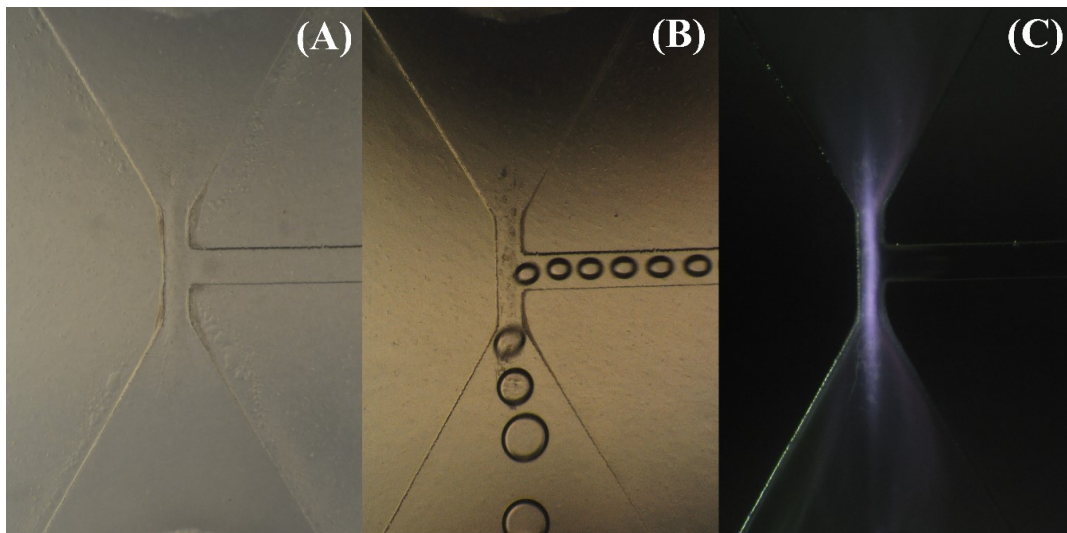


Figure 3.5 Optical microscopy images of narrow channel in every experimental steps. LEP channels (A) before bubble generation, (B) after bubble generation, and (C) during plasma generation.

Figure 3.6 compares channel damage when different gases were introduced during DC-LEP and AC-LEP. The DC-LEP samples (Fig. 3.6A and B) showed less channel damage when gas was introduced. As before, the AC-LEP (Fig. 3.6C and D) samples showed much less channel damage than the DC-LEP ones, where the least damage was observed when argon gas was introduced. Figure 3.6E summarizes the volume percentage of channel expansion with and without gas introduction. There was an obvious difference between the huge channel expansion of the DC-LEP sample (69.1%) and small channel expansion of the AC-LEP sample (3.32%), with Ar gas introduced. In addition, DC-LEP samples showed no observable difference in the damage between air and Ar gas introduction. The different damage behavior could be attributed to different plasma generation mechanisms in the DC-LEP and AC-LEP processes. In the case of DC-LEP, the plasma generated after Joule heating creates vapor bubbles and some time is required to remove remaining products from previous plasma generation; the pulses of the applied DC power may not correspond with the times when the introduced bubbles are present.

Synchronization of applied voltage and bubble generation will allow lower power (lower applied voltage) to generate plasma than in case of bubble generation from Joule heating. Therefore, the channel damage did not reduce significantly in the case of DC-LEP with gas introduction. In contrast, the AC power source can be applied continuously for a longer period compared to the DC source; hence, the generated bubbles are expected to remain inside the narrow channel for a longer period, stabilizing the plasma. Hence, introduction of bubbles could greatly facilitate plasma generation.

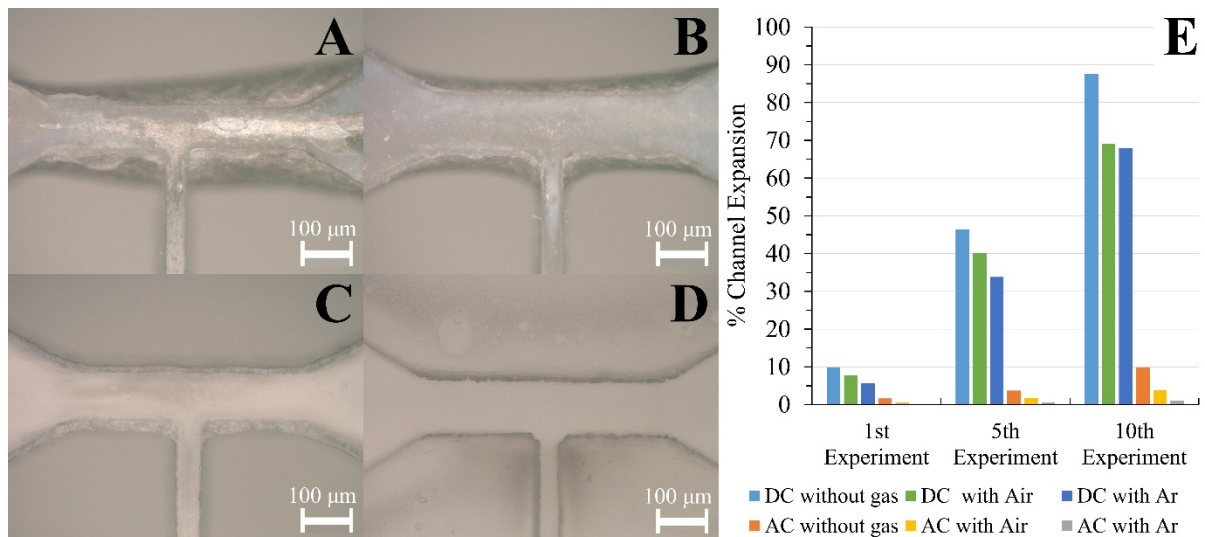


Figure 3.6 Optical microscopy images of chips used under different condition. (A) DC-LEP with air, (B) DC-LEP with Ar, (C) AC-LEP with air, and (D) AC-LEP with Ar. (E) Comparison of channel expansion in DC-LEP and AC-LEP during the different experiments.

3.4 Investigation of effects of gas introduction

Typically, AC-LEP without gas introduction requires an incubation time before bubbles (and therefore, plasma) is generated from outside of narrow channel. To clarify the effect and importance of the incubation time, gas was intentionally introduced during LEP experiments.

Nitrogen and oxygen gas were selected as two further candidates for generation of bubbles; nitrogen gas can be produced from atomization of the nitric acid solvent, while oxygen is a product of the hydrolysis of water. In the case where no gas was introduced, the first plasma generation was observed after 15 s. On the contrary, plasma was generated almost immediately after turning on the power source when air or nitrogen was introduced, and after 1 s or 2 s when Ar or oxygen gas was used. In addition, for AC-LEP without gas introduction, adequate range of solution flow rate is narrow and low which is $30 \mu\text{L min}^{-1}$. [18] In contrast, DC-LEP shows better result at higher flow rate that is $100\text{-}1000 \mu\text{L min}^{-1}$. [13] From these results, we concluded that the externally introduced bubble is important factor for plasma generation in the AC-LEP system, where hydrolysis of water occurs during the incubation time and the bubbles accumulate and move to the narrow channel with adequate flow rate. Here, the gas acts as seed bubble, AC-LEP is generated by lower powers. These results suggest that the lower damage in conventional AC-LEP without gas introduction also attributes to H_2/O_2 bubbles generated by hydrolysis at electrodes and consequently introduced into the LEP from outside of narrow channel.

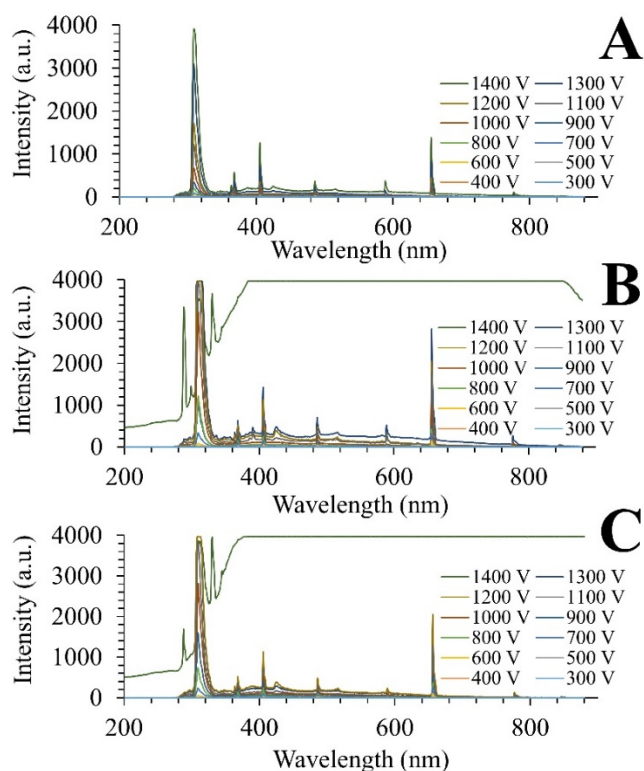


Figure 3.7 Comparison of voltage dependence. Emission spectra measured during DC-LEP (A) without gas introduction, (B) with air, (C) with Ar.

As reduced channel damage was observed when introducing gas during AC-LEP, we proposed that it might have a similar effect during DC-LEP with gas introduction. Therefore, air and argon were introduced during DC-LEP and the voltage dependence of the signal intensity was investigated. Fig. 3.7. Illustrated the emission spectra in all cases.

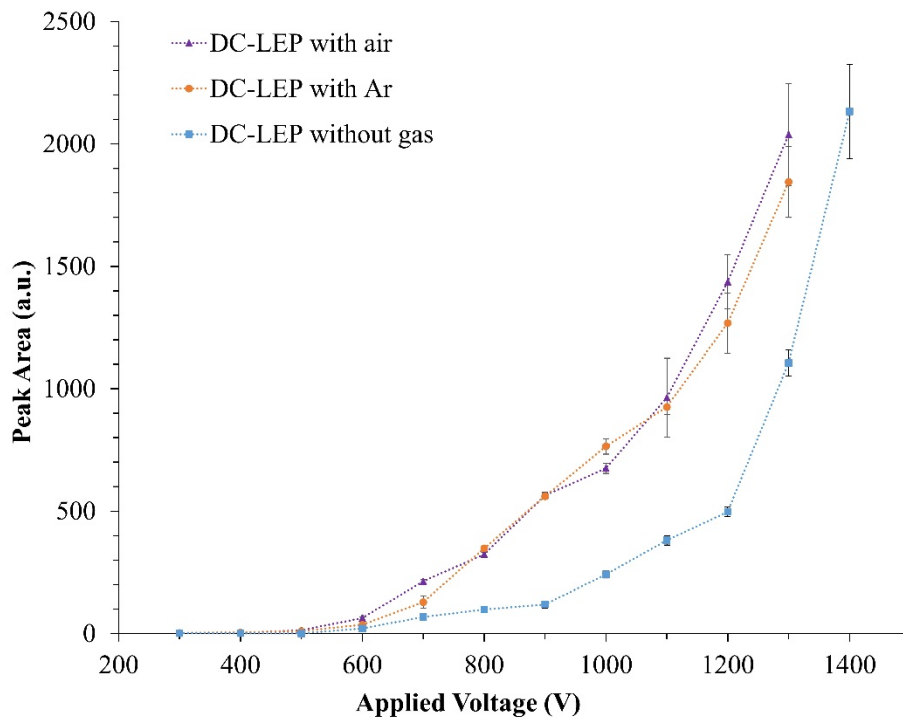


Figure 3.8 Comparison of voltage dependence. Calculated peak areas as a function of voltage for all cases.

Fig. 3.8 shows that the intensity of the Pb signal was higher when gases were introduced compared to the case of no gas at the same applied voltage, but no obvious difference between air and Ar was observed. This indicates that it is possible to apply a lower voltage (100–200 V lower) and obtain a comparable signal intensity when gas is introduced, which should reduce channel damage. These facts also suggest that the voltage required for bubble generation by homogeneous nucleation in the narrow channel is higher than that required for plasma generation. In conventional DC-LEP, a high-applied power is applied to generate bubbles, then the identical and constant voltage still applied for following plasma generation, which some part of applied power is an excess power for plasma generation resulting the higher damage in conventional DC-LEP. Under AC power conditions, the plasma appeared in the bubble grown from the externally introduced seed bubble. This enables bubble formation with lower applied

power, where plasma can be generated under milder conditions. Considering all of the experimental results, the proposed mechanism of low channel damage in AC-LEP is shown in Fig 3.9. It can be seen that a gas bubble produced at an electrode or by the external gas generation system reaches the narrow channel. Next, liquid electrode plasma appears inside of the gas bubble as a result of the applied voltage. Finally, the elements in solution enter the plasma and emit their characteristic optical emission lines for quantitative analysis.

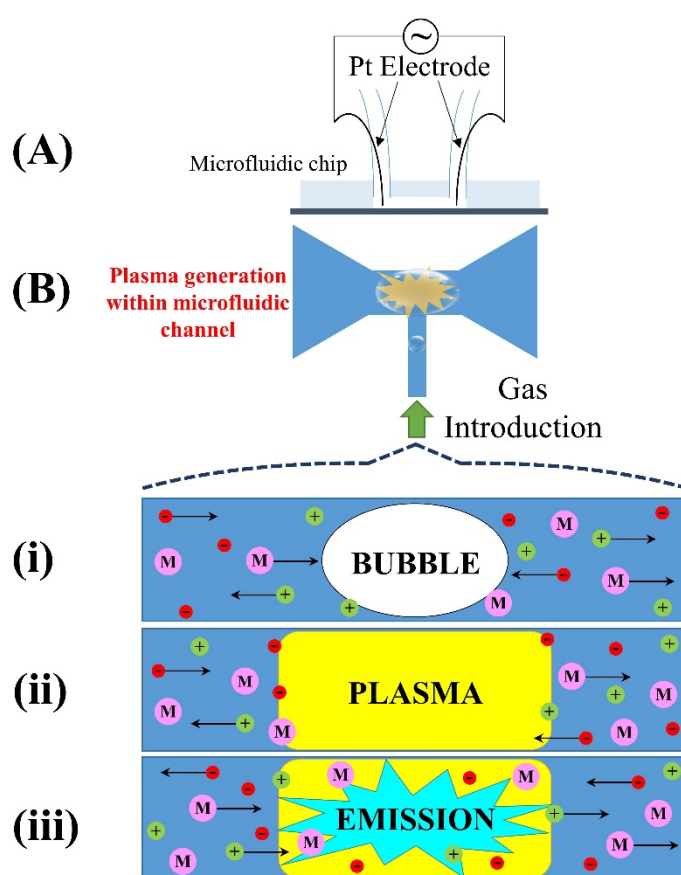


Figure 3.9 Schematic diagram showing the proposed mechanism of liquid electrode plasma.

(A) Side view of a LEP chip. (B) Top view of LEP channel and mechanism of plasma generation and optical emission. (i) A gas bubble reaches the narrow channel. (ii) Liquid electrode plasma appears within the gas bubble. (iii) Elements in solution enter the plasma and emit their characteristic optical emission lines for quantitative analysis.

3.5 Long time stability of AC-LEP emission signal with various gases

Long time stability of emission signals is one of the important factors for developing reliable elemental analysis methods. Hence, we introduced different gases during AC-LEP while monitoring the emission signal over time. Fig. 3.10 shows that, with gas introduction, the plasma could be generated over a longer time. Without gas introduction, after continuously applying a voltage to the narrow channel, the emission signal disappeared after around 40 min. When Ar gas was introduced, the emission signal showed the most stable average signal intensity. When other gases were used, we observed signals for up to 1 h, although the signal stability was lower than for Ar. This indicates that gas introduction reduces channel damage, leading to longer chip lifetimes. Interestingly, when air was introduced, the emission signal seemed to disappear around 10 min, and from 26 to 40 min, and showed huge fluctuations thereafter.

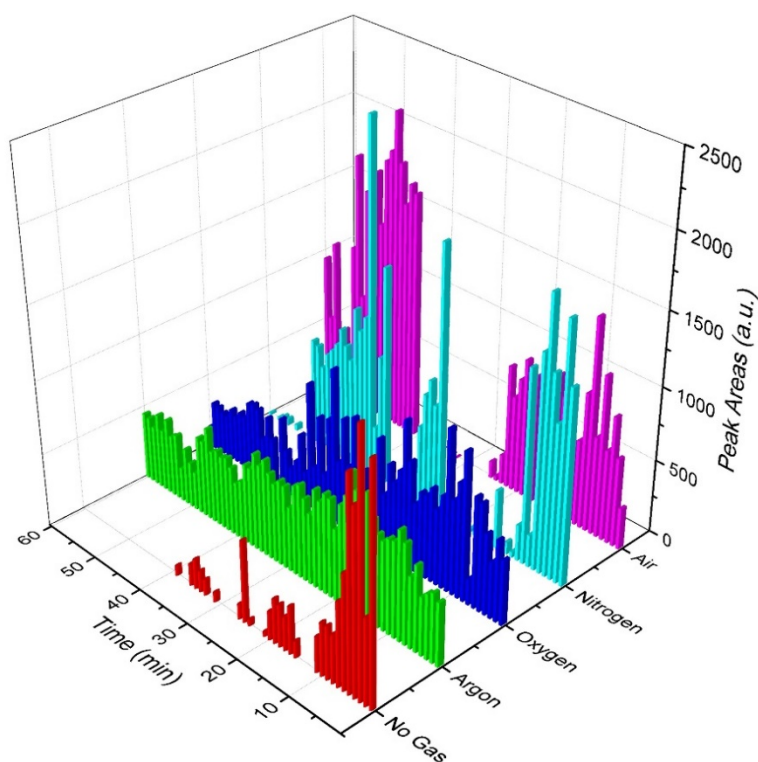


Figure 3.10 Spectroscopy peak areas for detecting Pb as a function of time and the type of gas introduced during AC-LEP

3.6 Measurement of excitation temperature and effects of introduced gases on excitation temperature

In this part, 50 mg L⁻¹ Fe in 0.1 M HCl with PDMS chip was analyzed. Applied voltage at 800 V was used with various types of gas introduction. Emission light at the center part was transferred to spectrometer (Andor Shamrock SR303i, focal length 0.303 m, diffraction grating of lines 2400 lines mm⁻¹) through optical fiber. Spectrum range of selected Fe(I) lines (Table 3.1) was from 362.2 to 389.5 nm. Spectroscopic data was obtained from the National Institute of Standards and Technology (NIST) Atomic Spectra Database.

Table 3.1 Spectroscopic data of the atomic Fe emission lines used in this work.

Line	Wavelength (nm)	Statistical weight	Transition probability (10 ⁷ s ⁻¹)	Excitation energy (10 ⁻¹⁹ J)
a	371.99	11	1.620	5.348
b	373.49	11	9.020	6.705
c	373.71	9	1.420	5.406
d	374.95	9	7.640	6.774
e	375.82	7	6.340	6.831
f	376.38	5	5.440	6.875
g	381.58	7	13.000	7.597

Figure 3.11 illustrated the observed spectrum and emission line (a-g) used corresponding to the spectroscopic data in Table 3.1. Typically, the excitation temperature was calculated from the slope of the linear fitting of a Boltzmann plot [19, 20].

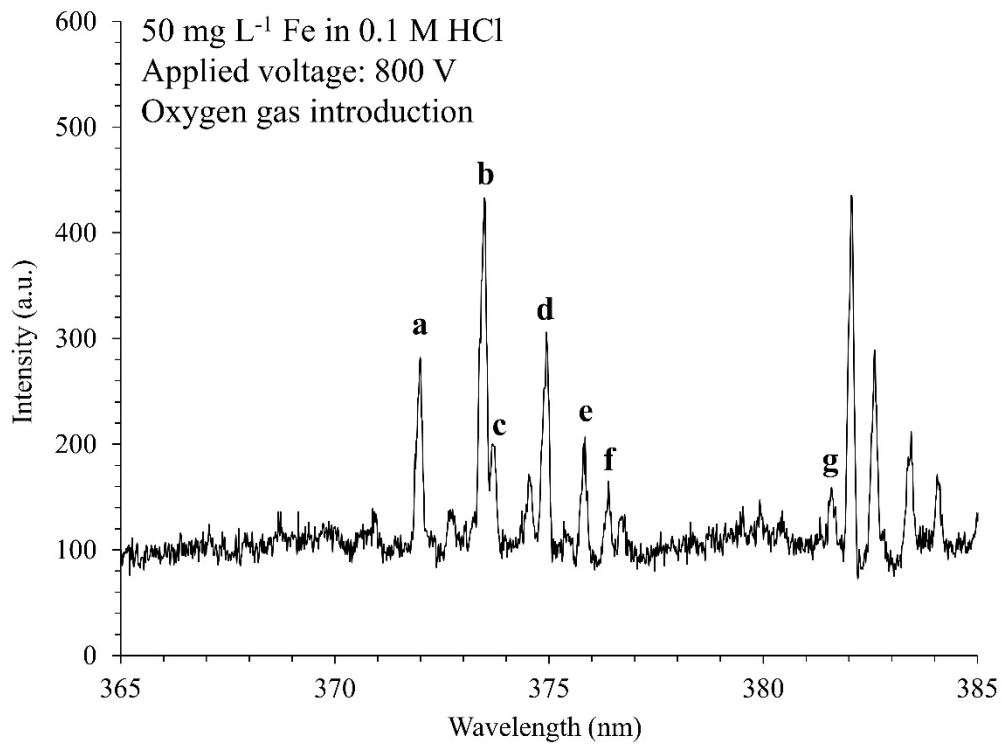


Figure 3. 11 Emission spectra of 50 mg L⁻¹ Fe in 0.1 M HCl of AC-LEP with oxygen gas introduction.

The Boltzmann plot relation is

$$\ln \frac{I_{nm}}{g_n A_{nm}} = -\frac{E_n}{kT} + C, \quad (1)$$

where I is the measured intensity, λ is the transition wavelength (nm), n denotes the lower level, m denotes the upper level, g is the statistical weight, A is the transition probability

(s-1), E is the energy (eV) of the upper level, k is Boltzmann's constant (eV K⁻¹), T is the excitation temperature (K), and C is constant.

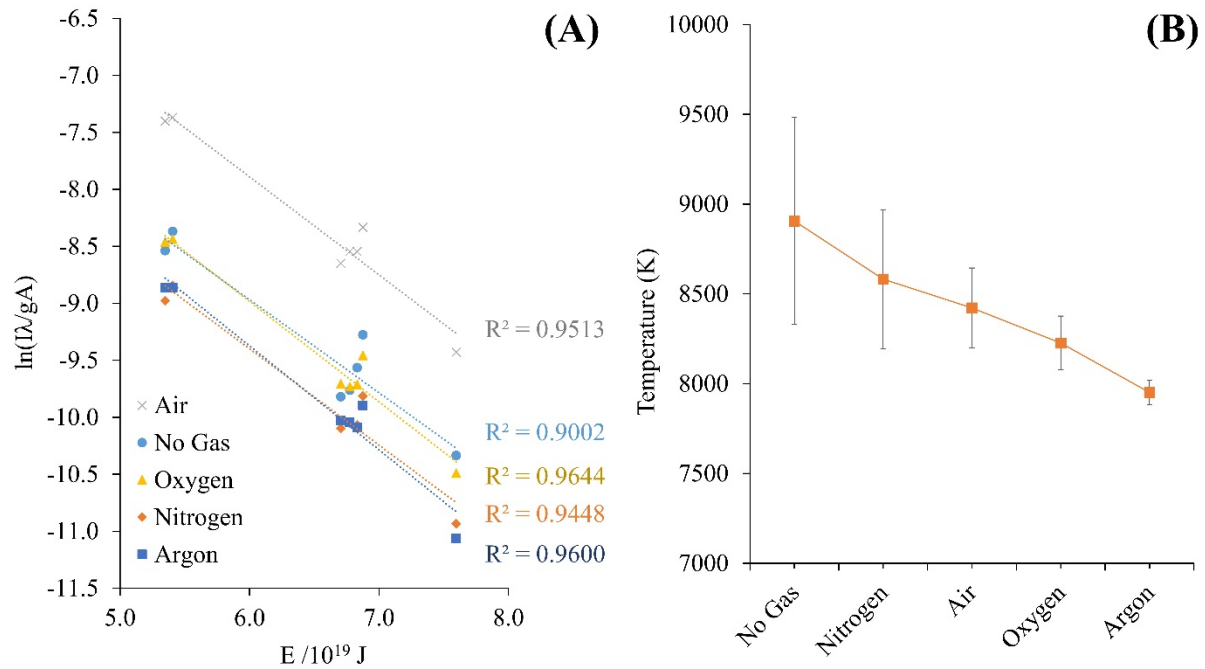


Figure 3.12 (A) Boltzmann plot obtained from AC-LEP spectrum and (B) effects of voltage applied and type of introduced gas on excitation temperature

Figure 3.12A illustrates a Boltzmann plot plotted based on Fig. 3.11. There is a satisfied correlation between $(I\lambda/gA)$ and the excitation energy E (eV), which is correlation coefficient range from 0.9002 to 0.9644. Consequently, the excitation temperature calculated from the graph was in the range of 8000 – 9000 K, in average. For AC-LEP, in case of argon gas introduction showed the lowest excitation temperature and without gas introduction case showed highest temperature with huge standard deviation. These results suggested that when gas was introduced, plasma could be generated easily compared to the case of without gas introduction. Small standard deviation suggested that with argon gas introduction, plasma was

stably generated. On the other hand, for DC-LEP, bubbles are generated from high power and no obvious difference in plasma temperature, as shown in Fig. 3.13. In the initial stage, only introduced gas case showed a main contribution for seed bubble and plasma generation. After that, water vapor will mix with introduced gas and bubble is generated. Thus, the effect of introduced gas was reduced because of mixture of gas and water vapor.

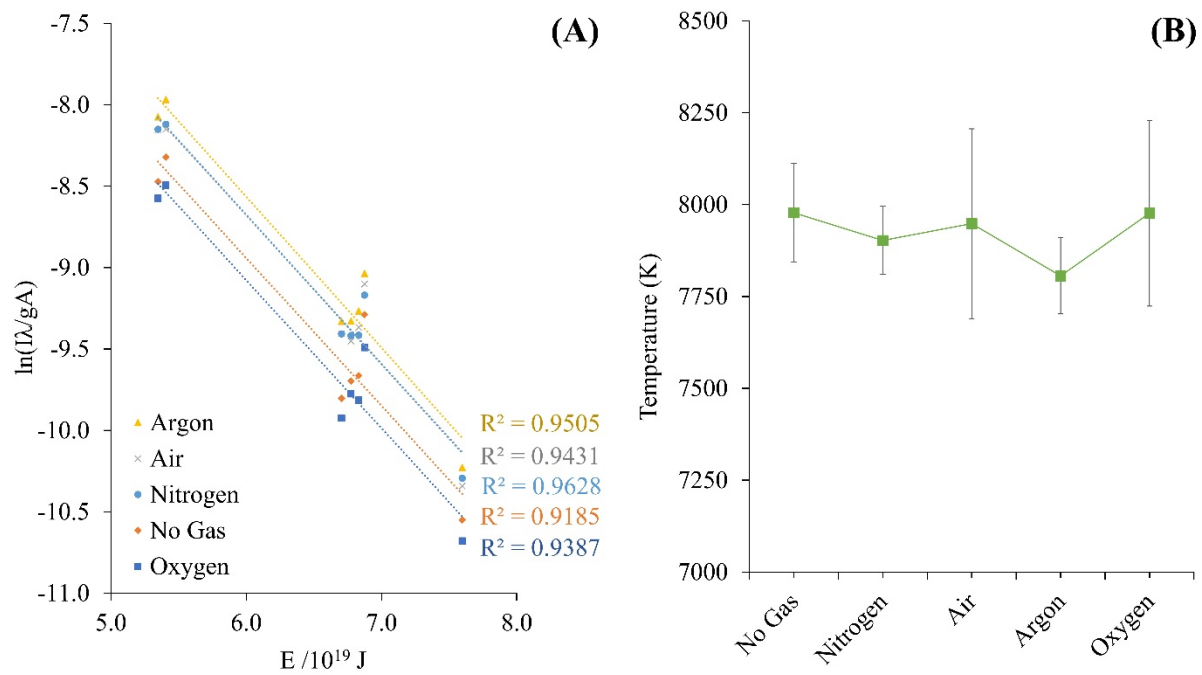


Figure 3.13 (A) Boltzmann plot obtained from DC-LEP spectrum and (B) effects of voltage applied and type of introduced gas on excitation temperature

These results of excitation temperature indicates that LEP as a light source of emission spectrometers provides sufficient power for elemental analysis. In fact, the excitation temperatures have been recorded to be 6000–8000K in ICP [21].

3.7 Analytical performance of AC-LEP

The analytical performance of AC-LEP with the introduction of different gases was studied using Pb as a model heavy metal analyte. Pb concentrations of 0–100 ppm in 0.1 M nitric acid were investigated. Fig. 3.14 shows the analyzed peak area as a function of Pb concentration, where the linear part of the curve for samples without gas introduction was shorter and become non-linear at Pb concentrations above 25 ppm. The slope of the calibration curve can be used to represent the detection sensitivity. The introduction of Ar gas resulted in the highest detection sensitivity, with a relatively low deviation and high coefficient of linear regression (R^2). Hence, we conclude that the introduction of gas bubbles facilitated the stability of plasma generation, while allowing the applied power to be reduced. Even though one of the advantages of LEP is that a gas does not need to be supplied, introduction of gas allowed us to elucidate some parts of the LEP mechanism and more clearly understand aspects of this novel plasma source for future applications.

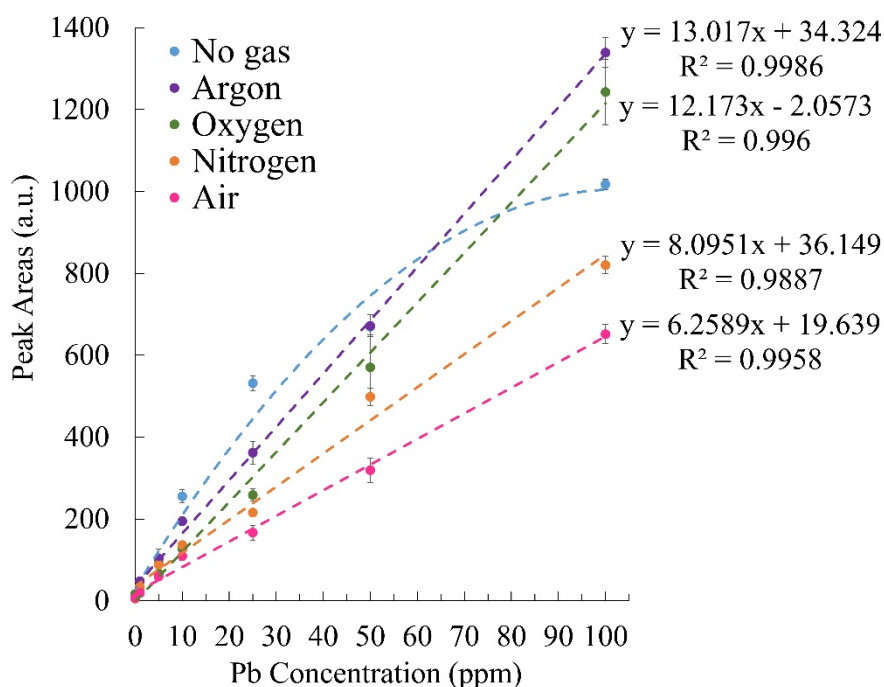


Figure 3.14 Analytical performance of AC-LEP with the introduction of different gases.

3.8 Conclusion

The effects of external gas introduction into AC-LEP and DC-LEP were studied. In AC-LEP, the introduction of gas into the channel resulted in the plasma starting almost immediately after the voltage was applied, while it started after several seconds without gas introduction. In both case of AC-LEP and DC-LEP, the external gas bubbles facilitated stable and high sensitive plasma generation with lower power, which result in reducing channel damage and increasing the lifetime of the analysis chip. These effects are significant in Ar introduction and AC-LEP cases. The power for homogeneous nucleation of bubble in conventional DC-LEP is higher than that required for plasma generation, resulting in high channel damage. Those facts suggest that the lower damage in conventional AC-LEP without gas introduction is attributed to H₂/O₂ bubbles generated by hydrolysis at electrodes and consequently introduced into the LEP from outside of narrow channel.

3.9 References

- [1] K. Greda, K. Swiderski, P. Jamroz, P. Pohl, Flowing Liquid Anode Atmospheric Pressure Glow Discharge as an Excitation Source for Optical Emission Spectrometry with the Improved Detectability of Ag, Cd, Hg, Pb, Tl, and Zn, *Anal Chem*, 88 (2016) 8812-8820.
- [2] C. Yang, D. He, Z. Zhu, H. Peng, Z. Liu, G. Wen, J. Bai, H. Zheng, S. Hu, Y. Wang, Battery-Operated Atomic Emission Analyzer for Waterborne Arsenic Based on Atmospheric Pressure Glow Discharge Excitation Source, *Anal Chem*, 89 (2017) 3694-3701.
- [3] L. Zheng, P. Kulkarni, Rapid Elemental Analysis of Aerosols Using Atmospheric Glow Discharge Optical Emission Spectroscopy, *Anal Chem*, 89 (2017) 6551-6558.

- [4] H. Zheng, X. Guan, X. Mao, Z. Zhu, C. Yang, H. Qiu, S. Hu, Determination of nitrite in water samples using atmospheric pressure glow discharge microplasma emission and chemical vapor generation of NO species, *Anal Chim Acta*, 1001 (2018) 100-105.
- [5] Q. He, Z. Zhu, S. Hu, H. Zheng, L. Jin, Elemental determination of microsamples by liquid film dielectric barrier discharge atomic emission spectrometry, *Anal Chem*, 84 (2012) 4179-4184.
- [6] T. Krahling, A. Michels, S. Geisler, S. Florek, J. Franzke, Investigations into modeling and further estimation of detection limits of the liquid electrode dielectric barrier discharge, *Anal Chem*, 86 (2014) 5822-5828.
- [7] R.M. Huang, Z.L. Zhu, H.T. Zheng, Z.F. Liu, S.C. Zhang, S.H. Hu, Alternating current driven atmospheric-pressure liquid discharge for the determination of elements with optical emission spectrometry, *Journal of Analytical Atomic Spectrometry*, 26 (2011) 1178-1182.
- [8] A. Leng, Y. Lin, Y. Tian, L. Wu, X. Jiang, X. Hou, C. Zheng, Pump- and Valve-Free Flow Injection Capillary Liquid Electrode Discharge Optical Emission Spectrometry Coupled to a Droplet Array Platform, *Anal Chem*, 89 (2017) 703-710.
- [9] D. Van Khoai, H. Miyahara, T. Yamamoto, P.T. Tue, A. Okino, Y. Takamura, Development of AC-driven liquid electrode plasma for sensitive detection of metals, *Japanese Journal of Applied Physics*, 55 (2016) 02BC23.
- [10] Y. Kohara, Y. Terui, M. Ichikawa, K. Yamamoto, T. Shirasaki, K. Kohda, T. Yamamoto, Y. Takamura, Atomic emission spectrometry in liquid electrode plasma using an hourglass microchannel, *Journal of Analytical Atomic Spectrometry*, 30 (2015) 2125-2128.

- [11] N.H. Tung, M. Chikae, Y. Ukita, P.H. Viet, Y. Takamura, Sensing technique of silver nanoparticles as labels for immunoassay using liquid electrode plasma atomic emission spectrometry, *Anal Chem*, 84 (2012) 1210-1213.
- [12] A. Iiduka, Y. Morita, E. Tamiya, Y. Takamura, Optical Emission Spectrometer of Aqueous Solution Samples Employing Liquid Electrode Plasma, in: J.N. Thomas Laurell, Klavs Jensen, D. Jed Harrison and Jörg P. Kutter (Ed.) 8th International Conference on Miniaturized Systems for Chemistry and Life Sciences, The Royal Society of Chemistry, Malmö, Sweden, 2004, pp. 423.
- [13] A. Kitano, A. Iiduka, T. Yamamoto, Y. Ukita, E. Tamiya, Y. Takamura, Highly sensitive elemental analysis for Cd and Pb by liquid electrode plasma atomic emission spectrometry with quartz glass chip and sample flow, *Anal Chem*, 83 (2011) 9424-9430.
- [14] Y. Kohara, Y. Terui, M. Ichikawa, T. Shirasaki, K. Yamamoto, T. Yamamoto, Y. Takamura, Characteristics of liquid electrode plasma for atomic emission spectrometry, *Journal of Analytical Atomic Spectrometry*, 27 (2012) 1457-1464.
- [15] S. Barua, I.M.M. Rahman, I. Alam, M. Miyaguchi, H. Sawai, T. Maki, H. Hasegawa, Liquid electrode plasma-optical emission spectrometry combined with solid-phase preconcentration for on-site analysis of lead, *J Chromatogr B Analyt Technol Biomed Life Sci*, 1060 (2017) 190-199.
- [16] V.K. Do, M. Yamamoto, S. Taguchi, Y. Takamura, N. Surugaya, T. Kuno, Quantitative determination of total cesium in highly active liquid waste by using liquid electrode plasma optical emission spectrometry, *Talanta*, 183 (2018) 283-289.
- [17] S. Barua, I.M.M. Rahman, M. Miyaguchi, A.S. Mashio, T. Maki, H. Hasegawa, On-site analysis of gold, palladium, or platinum in acidic aqueous matrix using liquid electrode plasma-optical emission spectrometry combined with ion-selective preconcentration, *Sensor Actuat B-Chem*, 272 (2018) 91-99.

- [18] K. Do Van, M. Hidekazu, Y. Tamotsu, T. Phan Trong, O. Akitoshi, T. Yuzuru, Development of AC-driven liquid electrode plasma for sensitive detection of metals, *Japanese Journal of Applied Physics*, 55 (2016) 02BC23.
- [19] J. Wang, B. Li, B. Gu, J. Zhang, X. Huang, J. Dong, H. Li, The Study on the Arc Plasma Temperature Measurement by Optical Emission Spectroscopy with Fiber Optical Transmission, *Spectroscopy Letters*, 31 (1998) 243-252.
- [20] M. Kumai, Y. Takamura, Excitation Temperature Measurement in Liquid Electrode Plasma, *Japanese Journal of Applied Physics*, 50 (2011) 096001.
- [21] N. Furuta, Spatial profile measurement of ionization and excitation temperatures in an inductively coupled plasma, *Spectrochimica Acta Part B: Atomic Spectroscopy*, 40 (1985) 1013-1022.

CHAPTER IV

METHOD DEVELOPMENT OF HEAVY METAL DETECTION BY ELECTRODEPOSITION COUPLED WITH LEP-OES

4.1 Introduction

Human have been widely used heavy metals for a long time ago, for example, metal plating plant, batteries, lead based paint, oilrig and sewage from steel mill. Although several adverse health effects of heavy metals have been known for a long time, exposure to heavy metals continues. Some of the heavy metal ions cause important environmental problems. The major threats to human health from heavy metals, such as lead, copper, cadmium, and mercury, are connected with exposure to them and accumulated in human body. Especially, a large amount of these toxic compounds are present in some surface and tap water due to the misuse of industrial wastes. World Health Organization (WHO) also concerned about this problems and studied their effects to human recently. Thus, it is important to look for a rapid, selective, sensitive, low-cost and simple technique for detection and monitoring all of these polluted substances in water.

In the past few years, the sensitive and selective detection of trace and ultra-trace levels heavy metal ions (HMIs) usually depended on traditional spectral methods, including, atomic absorption spectroscopy [1-3], inductively coupled plasma optical emission spectrometry [4-6], inductively coupled plasma mass spectrometry [7, 8], and total reflection X-ray fluorescence (TXRF) [9-11]. However, these spectrometric instruments still have some drawbacks, which are bulky, expensive, low sensitive and not suitable for on-site analysis [12,

13]. Although these spectrometry techniques have the advantages of high sensitivity and selectivity, it is still challenge to achieve determination in real environments that exhibit low concentration of HMIs.

Electrochemical detection (ECD) is very sensitive and capable of detecting in femtomole L^{-1} (10^{-15} M) range depending on the analyte and sample matrix. General experimental setup for electrochemical detection of HMIs normally comprises of an electrochemical cell consisting of an ionic conductor (an electrolyte) and an electronic conductor (an electrode). In this case, an aqueous solution consisting of HMIs serves as the electrolyte. The potential of electrochemical cell is measured at the interface of the electrode and electrolyte solution. The combination of electrochemical methods with spectral methods is reported to be competent of the determination of trace HMIs with high selectivity and sensitivity. Obviously, electrochemical spectral methods united the benefit of both electrochemistry and spectrometry [14]. Before the detection of specific heavy metals, sample solution to be measured can be separated and enriched by electrochemical methods, which tremendously improves the sensitivity and limit of detection of individual spectral methods. At the same time, comparing electrochemical methods solely, electrochemical spectral techniques overcome severe interference of coexist metals in the contaminants. There is a possibility that the costs of required equipment used in electrochemical spectral method increased, which may limit its usable range. However, LEP detector is relatively affordable price and portable size that will be unique advantage in facing of on-site and upcountry area monitoring and complex samples, and it may achieve simultaneous detection of coexisted heavy metals. Therefore, it is quite important to give an overview of electrochemical spectral methods. In this part, the combination of two techniques for heavy metal detection was studied. With the aid of deciding on the excellent utilized voltage for the oxidation/reduction potential and properties of the working electrode, an extra selectivity of detecting condition can be acquired. Target

compounds (analytes) are separated using a specific voltage in reduction reaction process. After separation, the compounds present at working electrode will be directly desorption and detection by using LEP.

4.2 Design of microchip for new detection system

The reaction chamber was fabricated by PDMS and glass substrate. After PDMS sheet fabrication, 3-mm diameter hole was punched on 1 cm² PDMS sheet. Glass substrate was cleaned with ethanol prior bonding with PDMS. Then, oxygen plasma treatment was used for bonding PDMS with hole onto substrate and covered with other PDMS layer. Working electrode and counter electrode are platinum wire with 0.3 mm diameter. For working electrode, PDMS was coated except for the area that will use for analyte deposition. After baking in the oven for 1.5 hr, the tip of electrode was cut to ensure clear electrode surface and to increase fabrication reproducibility. For efficiency comparison, Au wire was selected to be working electrode with same fabrication and usage. The reaction chamber is shown in Fig. 4.1. Below the chamber, fiber optic was applied to obtain the detection signal after electrodeposition. In the LEP detection step, DC-LEP with 200-1500 V of applied voltage with 0.5 msec on-time and 2 msec off-time was applied for 20 cycles. Analyte model in this study is 50 ppm Pb in nitric acid and HMIImBr. For the characterization of electrodeposition of target heavy metal, Energy Dispersive Spectrometer (EDS) (Tabletop Microscope TM3030, Hitachi, Japan) attachment for scanning electron microscope for chemical analysis was performed. Electrodeposition was achieved by using Potentiostat (Metrohm Autolab, Netherlands).

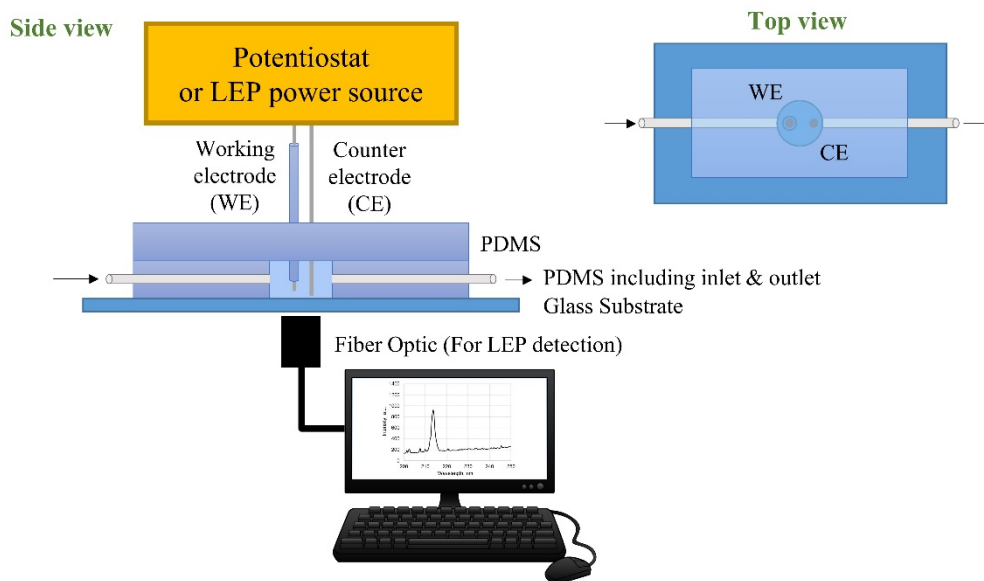


Figure 4.1 Reaction chamber and experimental setup for heavy metal detection by electrodeposition coupled with LEP-OES

4.3 Characterization of electrodeposition coupled with LEP-OES

From previous study, solution system and some experimental conditions were used as starting conditions. The solution flow rate of $100 \mu\text{L min}^{-1}$ and 0.1 M HNO_3 as solvent were applied in the first attempt of this new combination techniques. In the electrodeposition technique, -1 V was used as applied voltage constantly for 20 minutes. Figure 4.2 showed the EDS images of working electrode and elemental mapping of Pt and Pb. The preliminary results showed that with these Pb was successfully deposited onto the working electrode.

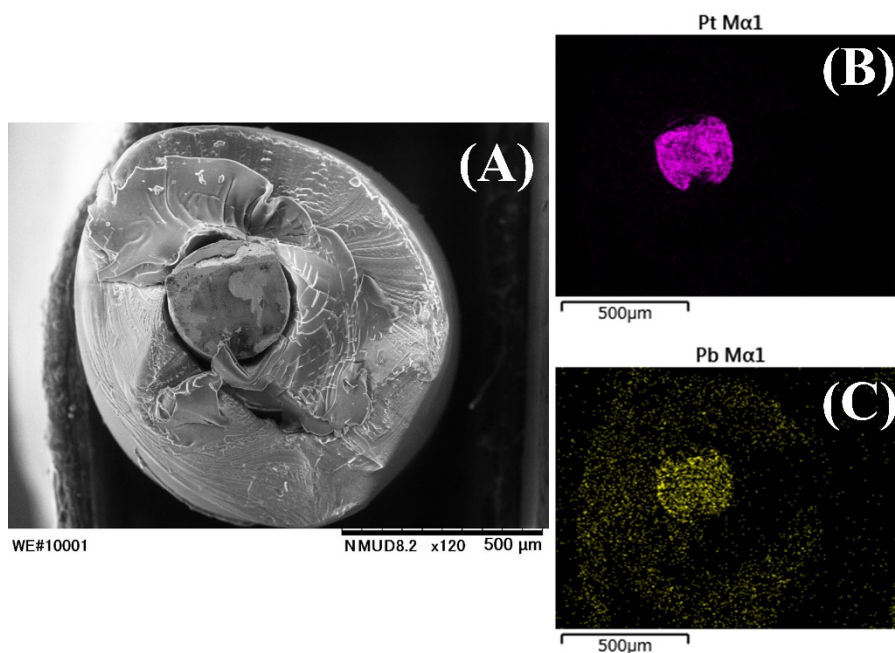


Figure 4.2 EDS imaged of (A) Pt working electrode after Pb deposition and elemental mapping of (B) Pt and (C) Pb

After that, LEP was performed to check the dissolution of Pb on the electrode. Figure 4.3 was illustrated the emission spectra of LEP after electrodeposition. Unfortunately, the emission peak of Pb at around 405 nm was not found. There might come from not enough amount of Pb deposited on the electrode, LEP dissolution step was not successful or the concentration of Pb dissolution to solution was lower than LOD. Moreover, there was also a possibility that HNO₃ itself was re-dissolved deposited Pb back to solution before LEP, therefore the optimization of experimental conditions was performed to improve detection sensitivity.

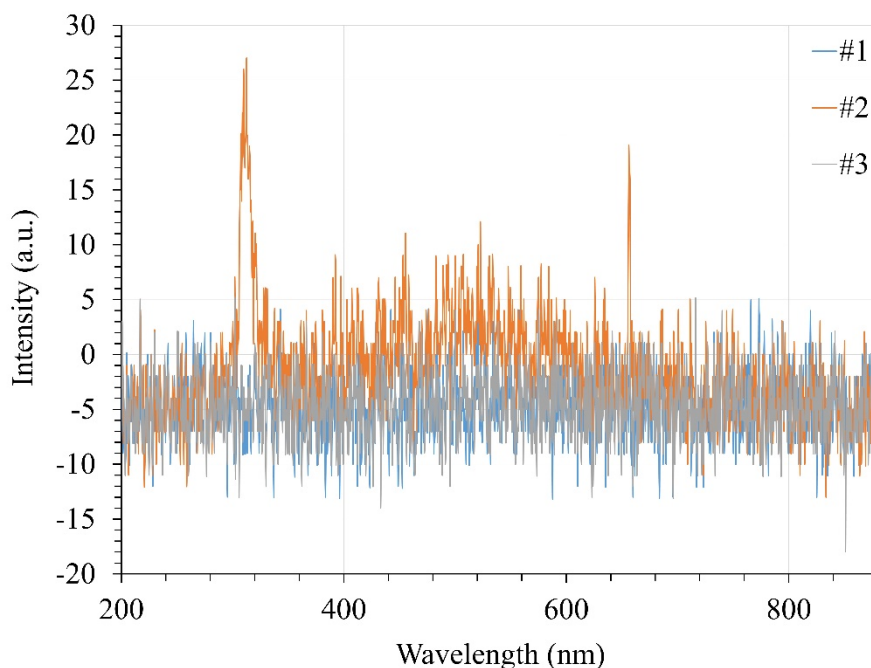


Figure 4.3 Emission spectrum of LEP after Pb deposition ($n = 3$). Experimental conditions: solution flow rate of $100 \mu\text{L min}^{-1}$, solvent of 0.1M HNO_3 , applied voltage of 900 V , on-time of 3 msec , off-time of 2 msec , and 50 cycles for one pulse (20 times repetition for one spectra)

4.4 Optimization of experimental conditions

This new HMIs detection platform still required many parameters to obtain optimized condition. First of all, from previous problem of solvent solution, polar aprotic solution without interference from spectra of cation of metal salt might be a better candidate for solvent in both electrodeposition and LEP. One of the interesting chemical was ionic liquids (ILs) water solution. Because of salt properties in the liquid state, ILs shows good intrinsic conductivity, low volatility, wide electrochemical windows, and high chemical and thermal stability [15-17]. In this work, 1-hydroxyethyl-3-methyl imidazolium bromide (HMImBr) was selected as solvent. The structure of HMImBr was shown in Fig. 4.4

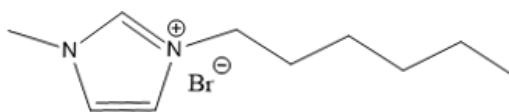


Figure 4.4 Chemical structure of 1-hexyl-3-methylimidazolium bromide (HMImBr)

Next, HMImBr was used to prepared Pb standard solution and tested with of DC-LEP with previous chip design. The result was shown that, with new solvent system, Pb emission peak was found at the expected position, as shown in Fig. 4.5. This can confirm that HMImBr can be used as solvent for Pb determination with DC-LEP.

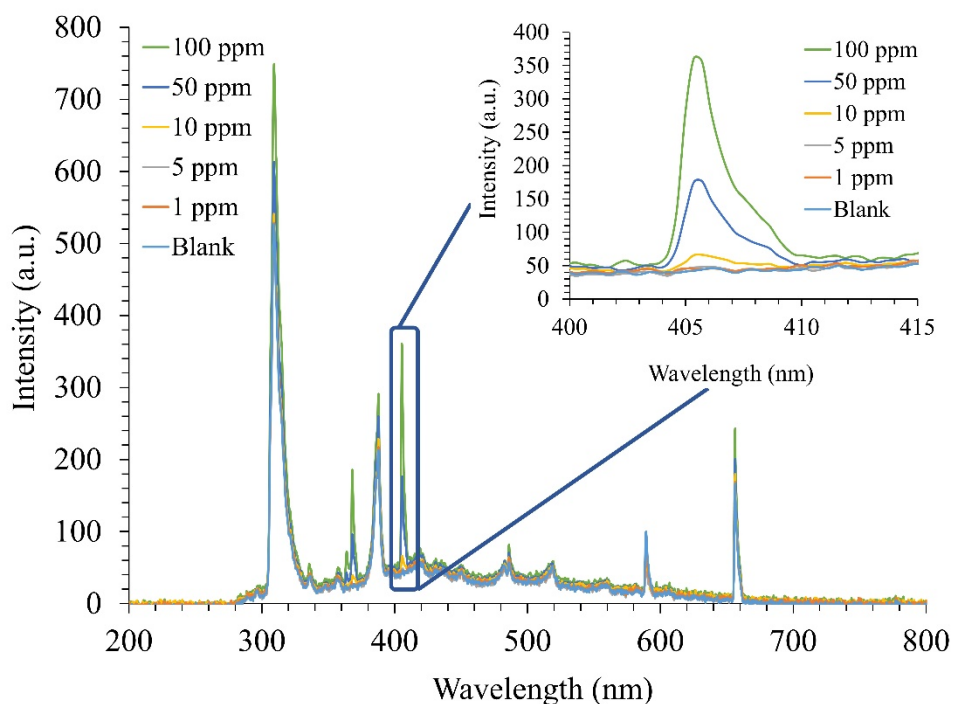


Figure 4.5 Emission spectra of standard Pb solution with concentration of 0 – 100 ppm in 0.1 M HMIMBr. Inset was zoom in at the peak position of 400-425 nm. Experimental conditions: solution flow rate of $100 \mu\text{L min}^{-1}$, applied voltage of 1500 V, on-time of 3 msec, off-time of 2 msec, and 20 cycles for one pulse (50 times repetition for one spectra)

Then, HMIMBr solvent was used in deposition step to examine Pb deposition on working electrode. Fig. 4.6 showed that this solution system exhibited the feasibility of Pb deposition, however the deposition efficiency still not good. From direct DC-LEP and deposition results, HMIMBr can be used as solvent for both deposition and LEP. However, the performance of this new detection system is needed to improve by further optimization.

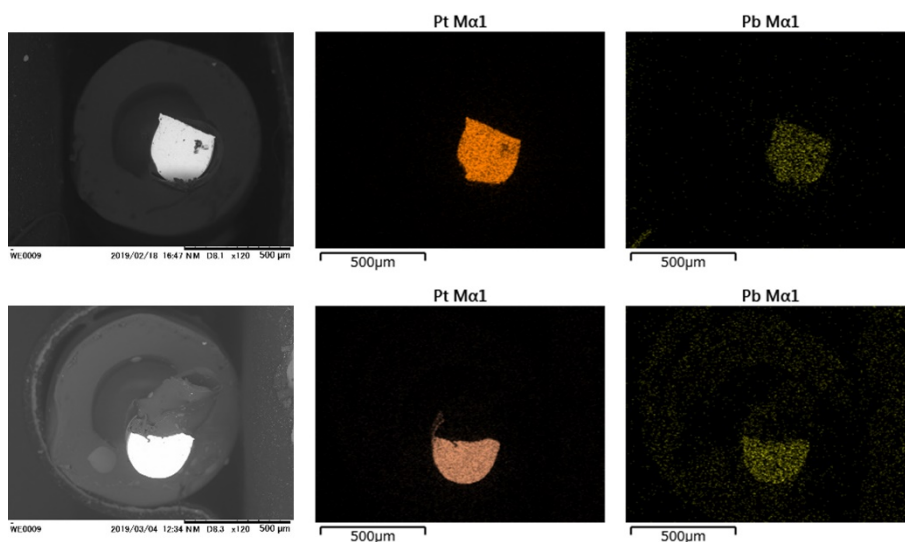


Figure 4.6 EDS images of Pt working electrode (above row) before Pb deposition and (below row) after Pb deposition. Experimental conditions: standard solution of 50 ppm Pb in 0.1 M HMImBr, solution flow rate of $100 \mu\text{L min}^{-1}$, and deposition potential of -1 V for 20 min.

In order to increase signal intensity, the experimental conditions must be investigated to achieve optimal conditions. To start with, deposition potential, the effect of deposition potential was evaluated from -1.5 V to -0.5 V with solution flow rate of $100 \mu\text{L min}^{-1}$ and deposition time of 20 minutes. Moreover, solvent type also studied in this experiment, which are 0.1 M HNO_3 , 0.1 M HMImBr, and 0.01 M HMImBr. From Fig.4.7 showed that with increasing applied potential, the amount of Pb was increase because of higher electrons was introduced to system and higher number of Pb ions can gain electron to form Pb^0 on the electrode surface. However, too high negative voltage can also caused hydrogen evolution that can interrupt smooth metal deposition. Thus, two more solutions also investigate in the same approach with this result.

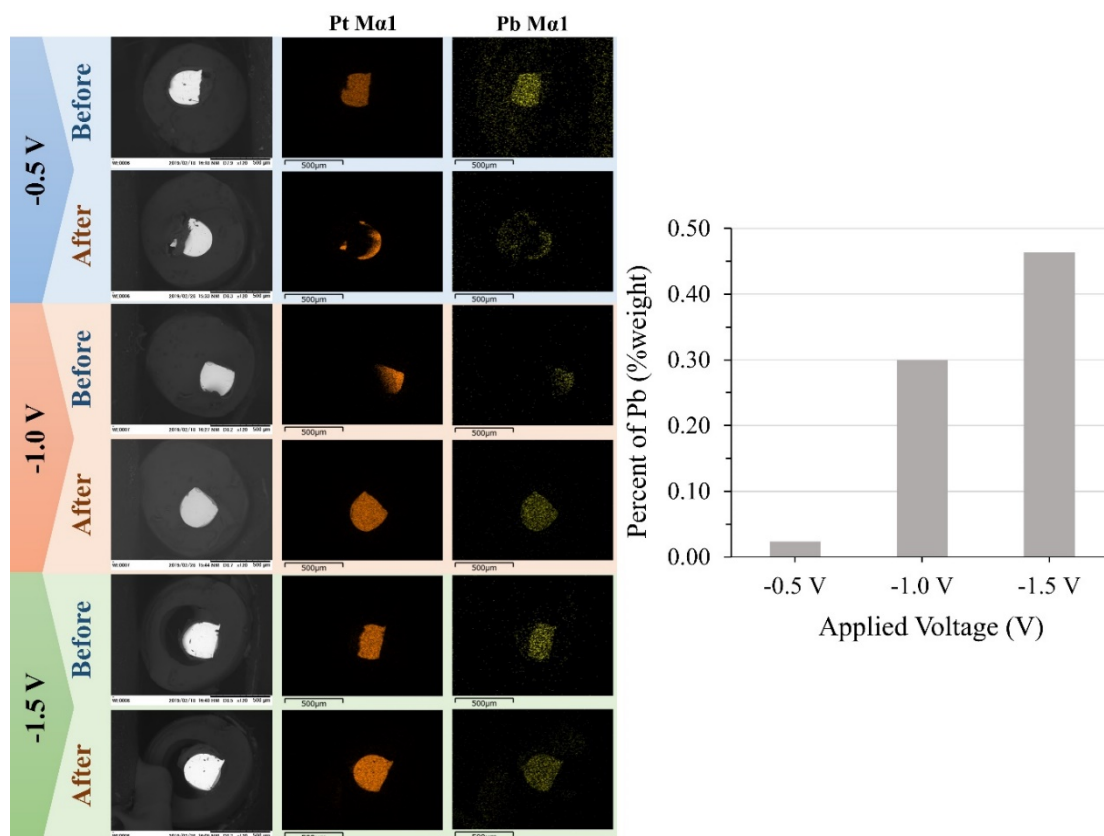


Figure 4.7 EDS images of Pt working electrode before and after Pb deposition and the elemental mapping of Pt (as working electrode) and Pb. Graph shown percentage of found deposited Pb on electrode surface at different deposition potential for 20 minutes. Sample solution is 50 ppm Pb in 0.1 M HNO₃.

Next, HMIImBr was used as solvent. Other experimental condition was same as previous results with different applied potential. As shown in Fig. 4.8, it is clearly seen that the increasing of amount of deposited Pb was directly proportional to more negative applied potential. In addition, the EDS image of -1.5V as deposition potential revealed obvious deposited Pb on electrode surface which the amount found even higher than that of 0.1 M HNO₃.

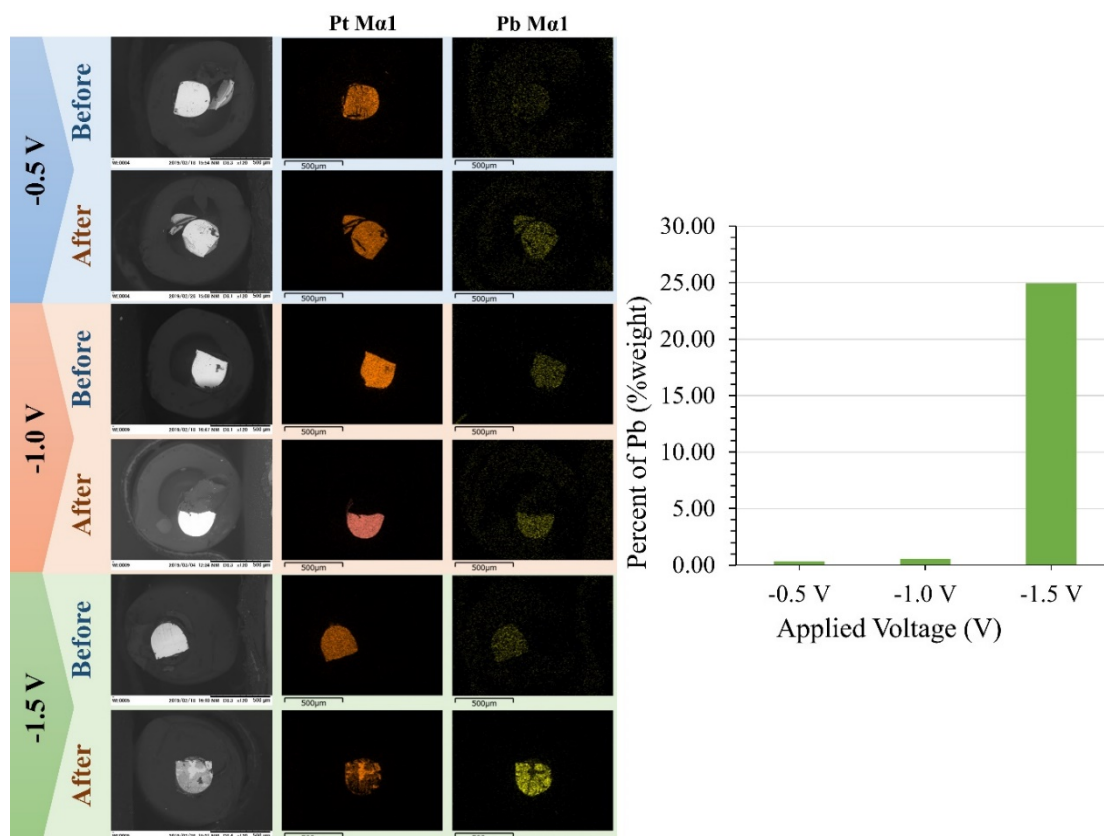


Figure 4.8 EDS images of Pt working electrode before and after Pb deposition and the elemental mapping of Pt (as working electrode) and Pb. Graph shown percentage of found deposited Pb on electrode surface at different deposition potential for 20 minutes. Sample solution is 50 ppm Pb in 0.1 M HMIImBr.

Lastly, we also performed the comparison HMIImBr concentration, that was 0.01 m HMIImBr, because ionic liquid is a high viscosity solution therefore it might be some hindrance from too viscous solution. The experiment was performed with same condition rather than the HMIImBr concentration. The results was consistent with previous results and the best deposition potential in this system also -1.5V, as shown in Fig. 4.9. The lower amount of deposited Pb may results of lower conductivity of solution due to low number of cations and anion in solution. Thus, the concentration of HMIImBr also affect to deposition efficiency. With all three different solution system, 0.1 M HMIImBr exhibited the highest amount of deposited

Pb. From these results, we can conclude that using 0.1 M HMImBr as solvent for Pb deposition is better than 0.1 M HNO₃ and 0.01 M HMImBr. Thus, 0.1 M HMImBr was selected as optimum solution in the next optimization.

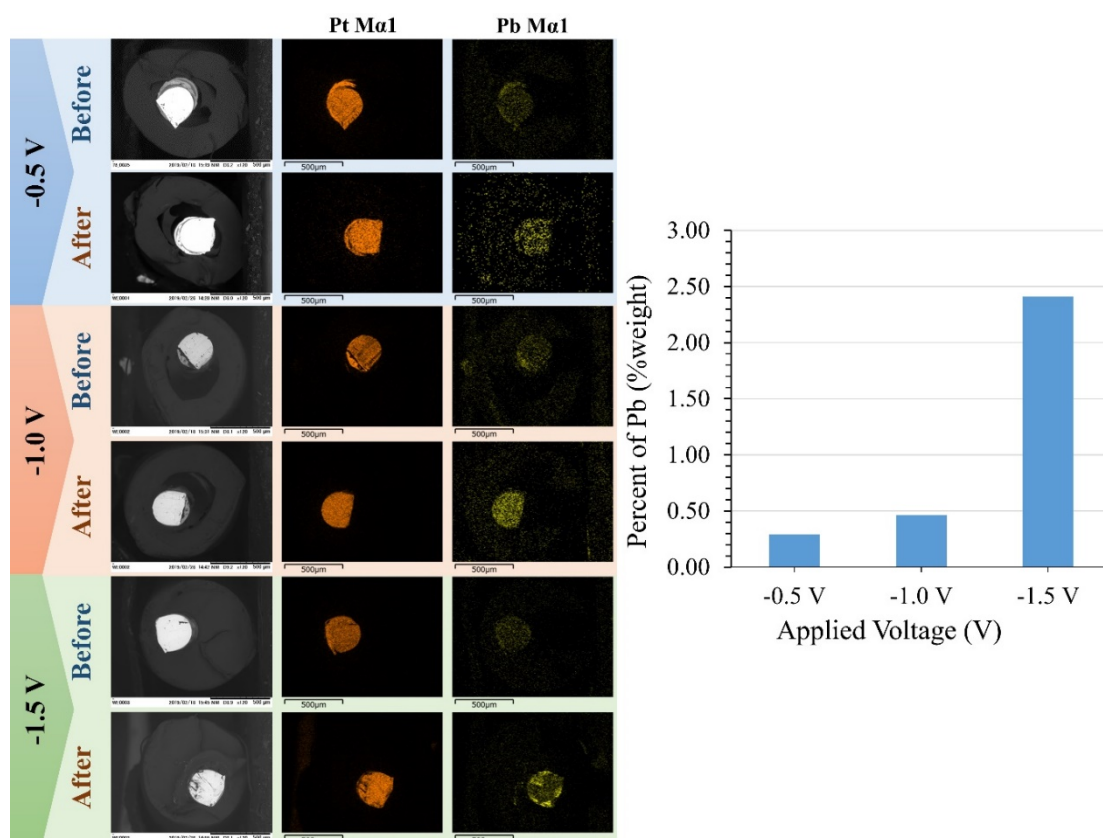


Figure 4.9 EDS images of Pt working electrode before and after Pb deposition and the elemental mapping of Pt (as working electrode) and Pb. Graph shown percentage of found deposited Pb on electrode surface at different deposition potential for 20 minutes. Sample solution is 50 ppm Pb in 0.01 M HMImBr.

Next, Au wire was carried out to compare the performance with Pt electrode. Generally, carbon-based electrode [18, 19] or metal nanoparticles [20-22] are used to modify working electrode for better determination performances. Gold electrode also one of the good materials

that used for metal detection because of wide potential window and robust materials. Thus, the working electrode was fabricated in the same procedure but used Au wire instead of Pt wire. The results showed that Au wire working electrode also showed same tendency with Pt wire working electrode, as shown in Fig. 4.10. These results suggest that Au wire can be used as working electrode as well as Pt wire with same experimental conditions (-1.5 V as deposition potential and 0.1 M HMImBr as solvent).

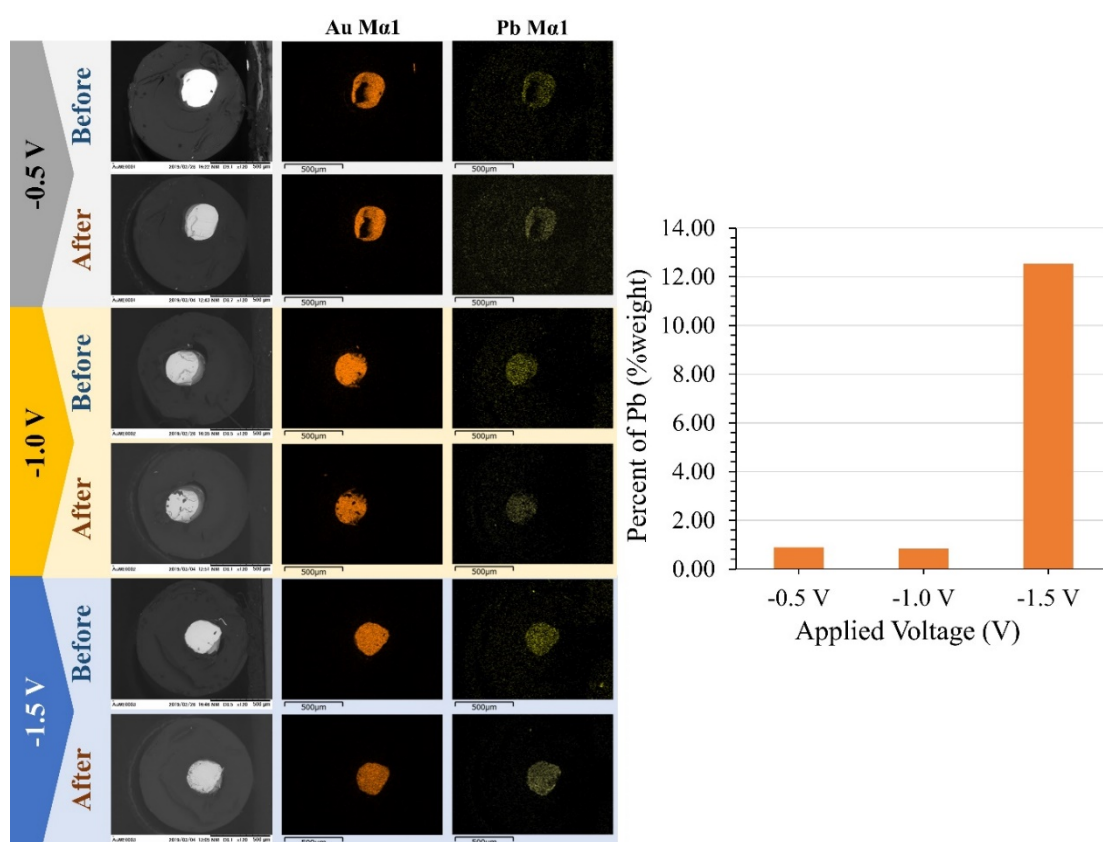


Figure 4.10 EDS images of Au working electrode before and after Pb deposition and the elemental mapping of Au (as working electrode) and Pb. Graph shown percentage of found deposited Pb on electrode surface at different deposition potential for 20 minutes. Sample solution is 50 ppm Pb in 0.1 M HMImBr.

After these preliminary results, the best experimental conditions of each working electrode was tested for LEP dissolution. From Fig. 4.11, we could clearly see that no Pb was found on working electrode surface after LEP applied to the detection system. This result can assure that LEP could directly remove deposited Pb from electrode surface. Then, the spectrum of LEP from this system was investigated, as shown in Fig. 4.12. From emission spectrum, Pb peak at 405.782 nm was not found. The reason may come from not enough amount of Pb of the dissolve Pb concentration was lower than LOD of LEP. In addition, the dissolution mechanism may different from assumption, which is not generated directly from working electrode surface, therefore the desired Pb peak was not appeared.

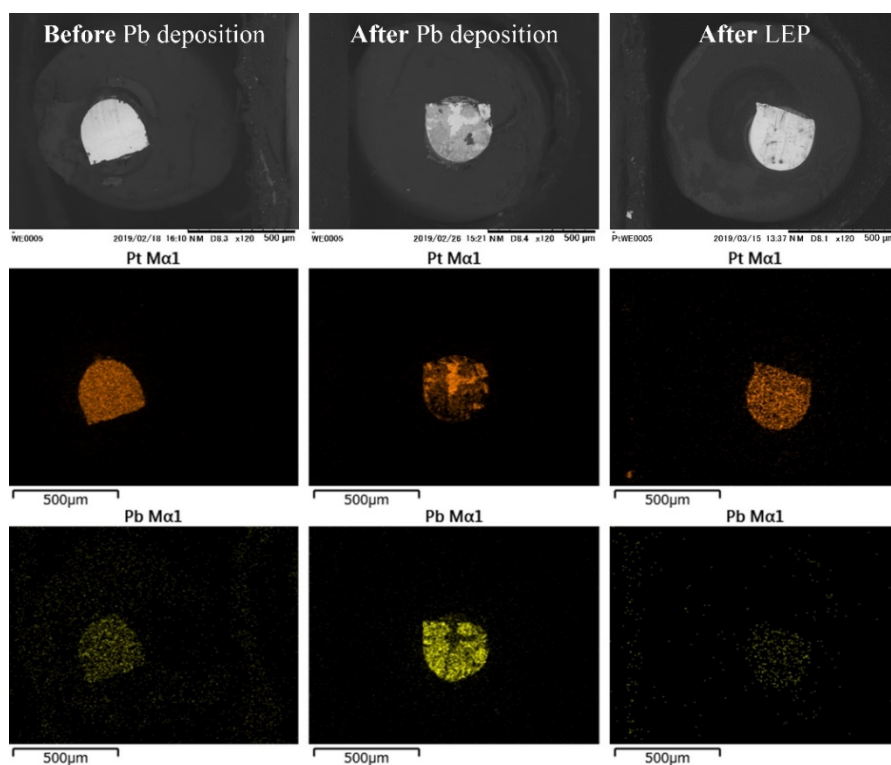


Figure 4.11 EDS images of Pt working electrode before, after Pb deposition, and after LEP dissolution and the elemental mapping of Pt (as working electrode) and Pb.

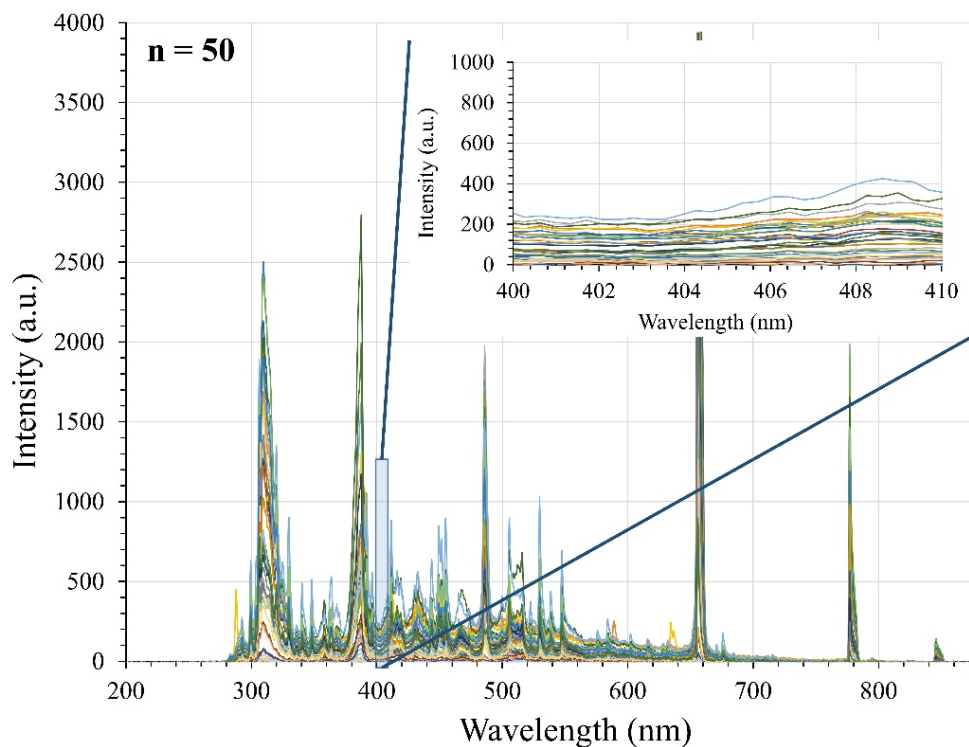


Figure 4.12 Emission spectra of deposited Pb on Pt working electrode with 0.1 M HMIMBr (flowing solution). Inset was zoom in at the peak position of 400-410 nm. Experimental conditions: solution flow rate of $100 \mu\text{L min}^{-1}$, applied voltage of 500 V, on-time of 0.5 msec, off-time of 2 msec, and 20 cycles for one pulse (50 times repetition for one spectra)

Likewise, Au wire working electrode was performed the same experiment as Pt wire working electrode. From Fig. 4.13, we could clearly observe that no Pb was found on working electrode surface after LEP applied to the detection system. This result can confirm that LEP could directly remove deposited Pb from electrode surface. Then, the spectrum of LEP from this system was also investigated, as shown in Fig. 4.14. From emission spectrum, Pb peak at 405.782 nm was found with relatively high signal. These results assured our assumption of the possibility of combination techniques. However, there is still not clear why Pb peak was not found in LEP. Thus, Au wire working electrode with previous optimized conditions will be used for further optimization.

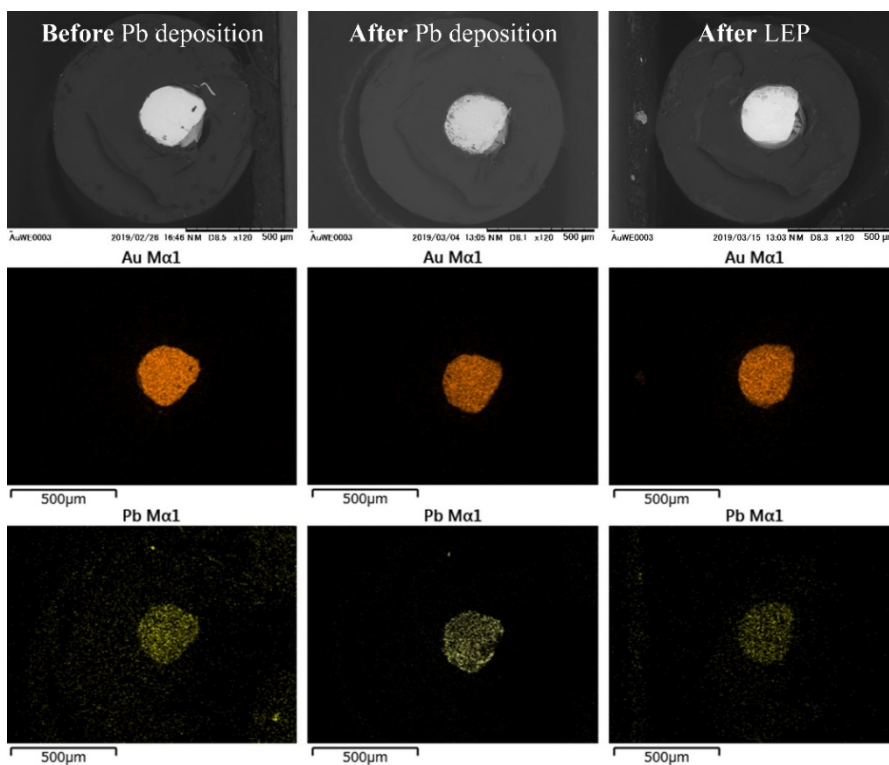


Figure 4.13 EDS images of Au working electrode before, after Pb deposition, and after LEP dissolution and the elemental mapping of Au (as working electrode) and Pb.

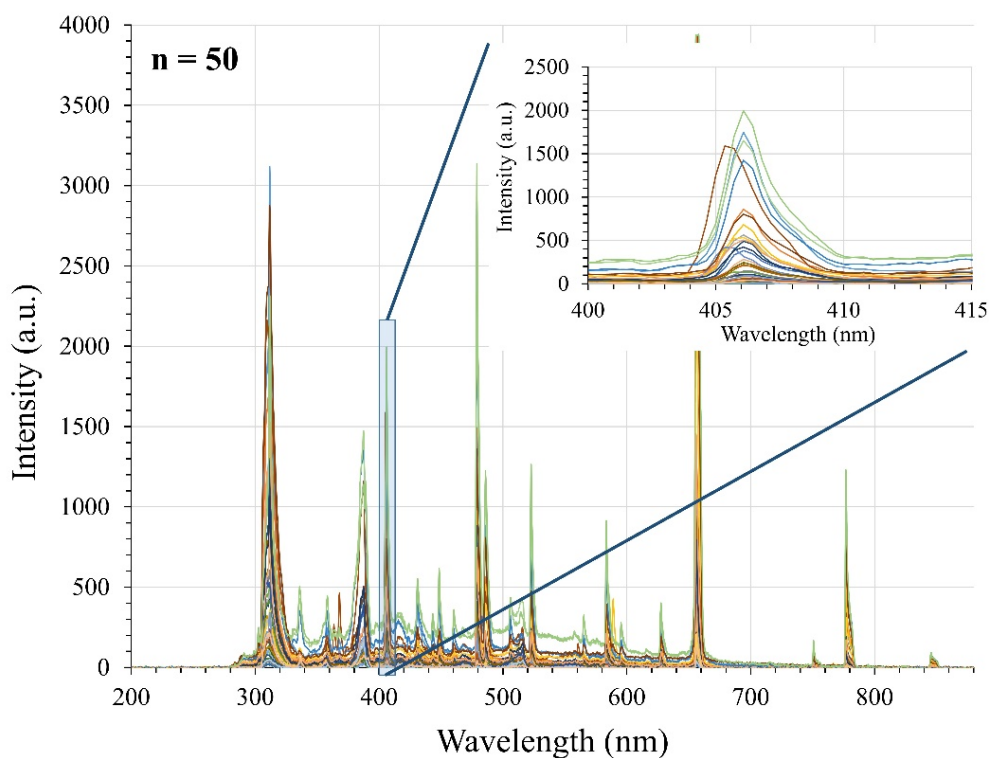


Figure 4.14 Emission spectra of deposited Pb on Au working electrode with 0.1 M HMIMBr (flowing solution). Inset was zoom in at the peak position of 400-410 nm. Experimental conditions: solution flow rate of $100 \mu\text{L min}^{-1}$, applied voltage of 500 V, on-time of 0.5 msec, off-time of 2 msec, and 20 cycles for one pulse (50 times repetition for one spectra)

Next, deposition time was investigated in range of 0 – 30 minutes. Longer deposition time will provide higher time of reduction of analyte on the working electrode. From Fig. 4.15, the amount of deposited Pb was increase when deposition time is increase. At 30 minutes of deposition time showed the highest amount of deposited Pb. After that, LEP was performed to observe the dissolution of Pb from electrode. The result showed the consistent tendency with the found Pb on electrode, as shown in Fig. 4.16. The highest peak area came from the electrode that found highest Pb. We can conclude that the optimum condition for these couple technique are Au wire as working electrode and solution was prepared from 0.1 M HMImBr.

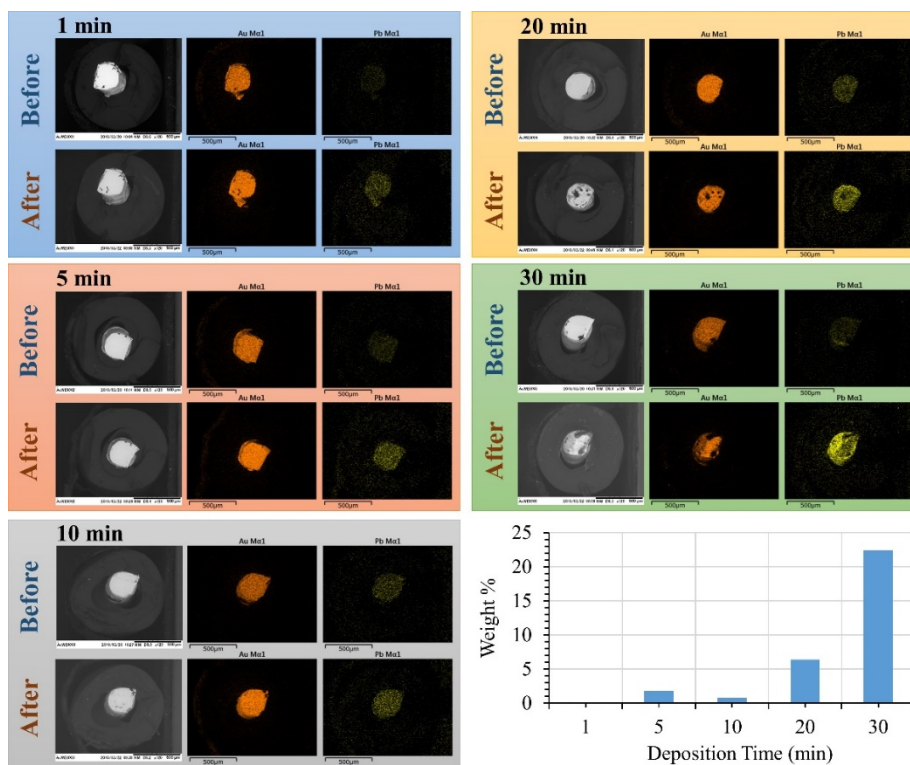


Figure 4.15 EDS images of Au working electrode before and after Pb deposition and the elemental mapping of Au (as working electrode) and Pb. Graph shown percentage of found deposited Pb on electrode surface at deposition potential of -1.5V with different deposition time. Sample solution is 50 ppm Pb in 0.1 M HMImBr.

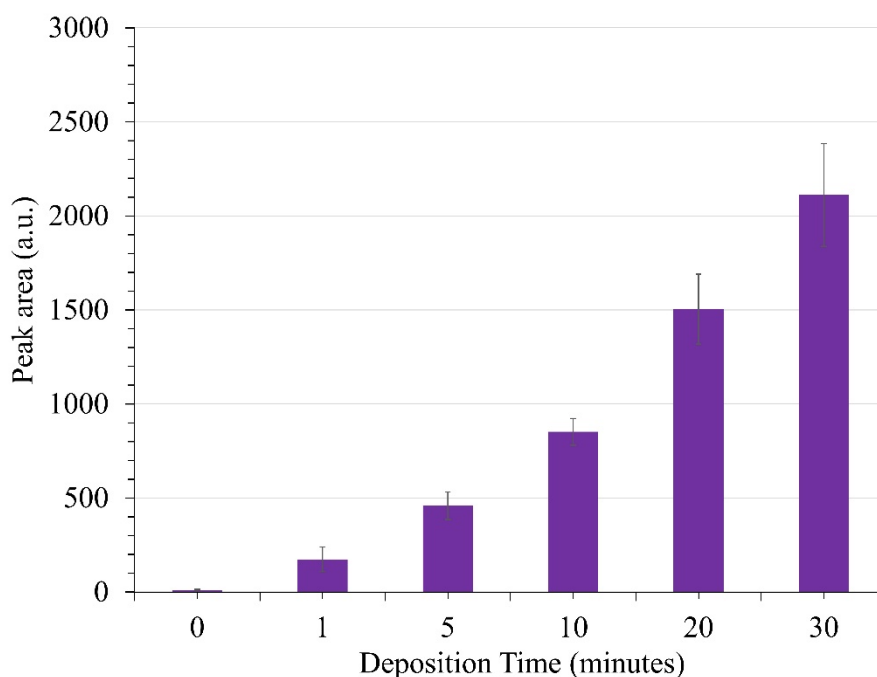


Figure 4.16 Effect of deposition time in range of 0 to 30 minutes. Experimental conditions: 50 ppm Pb in 0.1 M HMImBr solution flow rate of $100 \mu\text{L min}^{-1}$, applied voltage of 500 V, on-time of 0.5 msec, off-time of 2 msec, and 20 cycles for one pulse (50 times repetition for one spectra)

After some experimental parameters optimization, calibration curve and limit of detection was fabricated and calculated, as shown in Fig 4.17. The result shown that peak area was increasing with increasing of lead concentration, however, at very high concentration, it reached signal saturation. Due to the limitation of electrode surface area, after some concentration will not be able to deposit onto surface. Thus, the linear dynamic range from this calibration curve is 0 – 10 ppm of lead concentration. Within linear range, peak area is directly proportional to the lead concentration and illustrates satisfied linear regression ($R^2 = 0.9992$). The detection limit (LOD) of this system is 0.0279 ppm of lead, which was calculated from $3 \times \text{SD of blank} / \text{slope of calibration curve}$. In addition, there are still many parameters that needs

to be optimized to achieve the best situation for long time monitoring of heavy metal in real water sample.

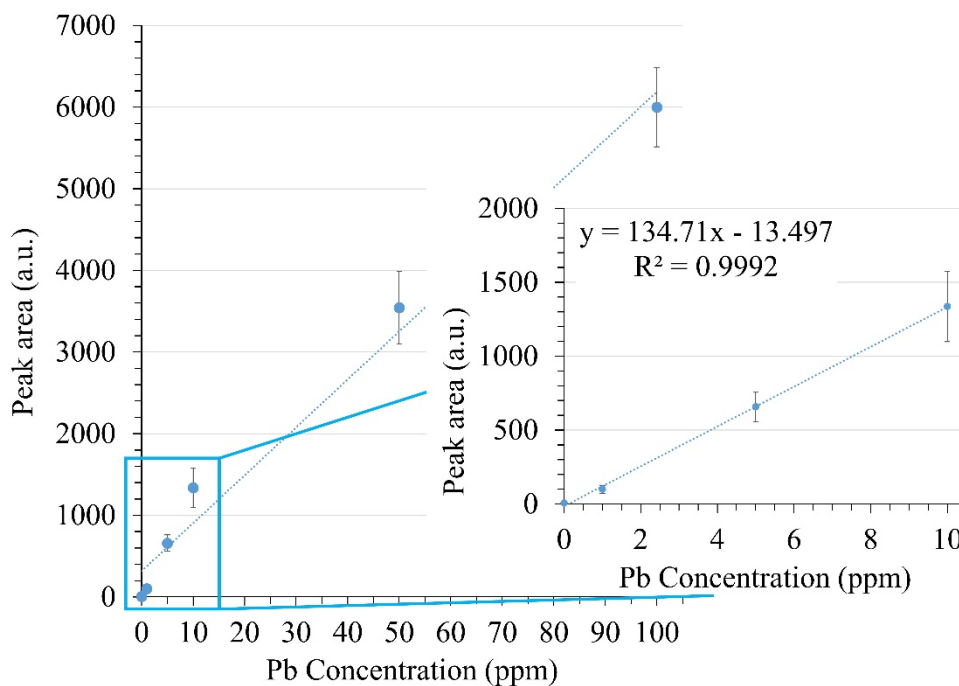


Figure 4.17 Analytical performance of electrodeposition coupled with LEP-OES of 0 – 100 ppm of lead in 0.1 M HMIImBr. Experimental conditions: solution flow rate of 100 $\mu\text{L min}^{-1}$, applied voltage of 500 V, on-time of 0.5 msec, off-time of 2 msec, 20 cycles for one pulse (50 times repetition for one spectra), and 3 times measurement for one data point.

4.6 Conclusion

In this part, we proposed new combination technique for long time environmental monitoring by using electrodeposition coupled with LEP-OES. By applied constant voltage, the analytes were deposited on electrode and after that, LEP would implement for direct plasma generation to detect deposited target analytes. EDS images confirmed our assumption and the feasibility of these new detection system. Next, some important experimental parameters were

optimized. Au wire was a better candidate for using as working electrode. The suitable solution is prepared from 0.1 M HMImBr, which is ionic liquid. Other experimental conditions are -1.5 V as deposition potential, 30 minutes as deposition time, 100 mL min⁻¹ as solution flow rate, applied voltage of 500 V, on-time of 0.5 msec, off-time of 2 msec, and 20 cycles for one pulse (50 times repetition for one spectra). With optimized condition, calibration curve was fabricated with the linear dynamic range of 0-10 ppm of lead and the calculated LOD is 0.3953 ppm. However, further optimization of experimental parameter and validation of this technique still need to be done in order to use for on-site analysis.

4.7 References

- [1] S. Khazaeli, N. Nezamabadi, M. Rabani, H.A. Panahi, A new functionalized resin and its application in flame atomic absorption spectrophotometric determination of trace amounts of heavy metal ions after solid phase extraction in water samples, *Microchemical Journal*, 106 (2013) 147-153.
- [2] M.A. Alvarez, G. Carrillo, Simultaneous determination of arsenic, cadmium, copper, chromium, nickel, lead and thallium in total digested sediment samples and available fractions by electrothermal atomization atomic absorption spectroscopy (ET AAS), *Talanta*, 97 (2012) 505-512.
- [3] M.T. Naseri, M.R. Hosseini, Y. Assadi, A. Kiani, Rapid determination of lead in water samples by dispersive liquid-liquid microextraction coupled with electrothermal atomic absorption spectrometry, *Talanta*, 75 (2008) 56-62.
- [4] C. Cui, M. He, B. Chen, B. Hu, Restricted accessed material-copper(II) ion imprinted polymer solid phase extraction combined with inductively coupled plasma-optical

- emission spectrometry for the determination of free Cu(II) in urine and serum samples, *Talanta*, 116 (2013) 1040-1046.
- [5] A. Beiraghi, S. Babaei, M. Roshdi, Simultaneous preconcentration of cadmium, cobalt and nickel in water samples by cationic micellar precipitation and their determination by inductively coupled plasma-optical emission spectrometry, *Microchemical Journal*, 100 (2012) 66-71.
- [6] L. Zhao, S. Zhong, K. Fang, Z. Qian, J. Chen, Determination of cadmium(II), cobalt(II), nickel(II), lead(II), zinc(II), and copper(II) in water samples using dual-cloud point extraction and inductively coupled plasma emission spectrometry, *J Hazard Mater*, 239-240 (2012) 206-212.
- [7] C.Y. Tai, S.J. Jiang, A.C. Sahayam, Determination of As, Hg and Pb in herbs using slurry sampling flow injection chemical vapor generation inductively coupled plasma mass spectrometry, *Food Chem*, 192 (2016) 274-279.
- [8] R.P. Lamsal, D. Beauchemin, Estimation of the bio-accessible fraction of Cr, As, Cd and Pb in locally available bread using on-line continuous leaching method coupled to inductively coupled plasma mass spectrometry, *Anal Chim Acta*, 867 (2015) 9-17.
- [9] N. Ullah, M. Mansha, I. Khan, A. Qurashi, Nanomaterial-based optical chemical sensors for the detection of heavy metals in water: Recent advances and challenges, *Trac-Trend Anal Chem*, 100 (2018) 155-166.
- [10] G.V. Pashkova, A.G. Revenko, A Review of Application of Total Reflection X-ray Fluorescence Spectrometry to Water Analysis, *Applied Spectroscopy Reviews*, 50 (2015) 443-472.
- [11] P. Wobrauschek, Total reflection x-ray fluorescence analysis—a review, *X-Ray Spectrometry*, 36 (2007) 289-300.

- [12] Y. Wei, C. Gao, F.L. Meng, H.H. Li, L. Wang, J.H. Liu, X.J. Huang, SnO₂/Reduced Graphene Oxide Nanocomposite for the Simultaneous Electrochemical Detection of Cadmium(II), Lead(II), Copper(II), and Mercury(II): An Interesting Favorable Mutual Interference, *J Phys Chem C*, 116 (2012) 1034-1041.
- [13] C. Gao, X.Y. Yu, R.X. Xu, J.H. Liu, X.J. Huang, AlOOH-reduced graphene oxide nanocomposites: one-pot hydrothermal synthesis and their enhanced electrochemical activity for heavy metal ions, *ACS Appl Mater Interfaces*, 4 (2012) 4672-4682.
- [14] B. Bansod, T. Kumar, R. Thakur, S. Rana, I. Singh, A review on various electrochemical techniques for heavy metal ions detection with different sensing platforms, *Biosens Bioelectron*, 94 (2017) 443-455.
- [15] D. Wei, A. Ivaska, Applications of ionic liquids in electrochemical sensors, *Anal Chim Acta*, 607 (2008) 126-135.
- [16] X. Huang, Y. Wang, X. Liao, B. Shi, Adsorptive recovery of Au³⁺ from aqueous solutions using bayberry tannin-immobilized mesoporous silica, *J Hazard Mater*, 183 (2010) 793-798.
- [17] A.M. Navarro-Suárez, J.C. Hidalgo-Acosta, L. Fadini, J.M. Feliu, M.F. Suárez-Herrera, Electrochemical Oxidation of Hydrogen on Basal Plane Platinum Electrodes in Imidazolium Ionic Liquids, *The Journal of Physical Chemistry C*, 115 (2011) 11147-11155.
- [18] L. Wang, X. Wang, G. Shi, C. Peng, Y. Ding, Thiocalixarene covalently functionalized multiwalled carbon nanotubes as chemically modified electrode material for detection of ultratrace Pb²⁺ ions, *Anal Chem*, 84 (2012) 10560-10567.
- [19] A. Mourya, S.K. Sinha, B. Mazumdar, Glassy carbon electrode modified with blast furnace slag for electrochemical investigation of Cu²⁺ and Pb²⁺ metal ions, *Microchemical Journal*, 147 (2019) 707-716.

- [20] T. Zhang, H. Jin, Y. Fang, J. Guan, S. Ma, Y. Pan, M. Zhang, H. Zhu, X. Liu, M. Du, Detection of trace Cd²⁺, Pb²⁺ and Cu²⁺ ions via porous activated carbon supported palladium nanoparticles modified electrodes using SWASV, *Materials Chemistry and Physics*, 225 (2019) 433-442.
- [21] J.H. Hwang, X.C. Wang, D.L. Zhao, M.M. Rex, H.J. Cho, W.H. Lee, A novel nanoporous bismuth electrode sensor for in situ heavy metal detection, *Electrochimica Acta*, 298 (2019) 440-448.
- [22] S. Dutta, G. Strack, P. Kurup, Gold nanostar electrodes for heavy metal detection, *Sensor Actuat B-Chem*, 281 (2019) 383-391.

CHAPTER V

GENERAL CONCLUSION

In this study, an elemental analyzer based on liquid electrode plasma optical emission spectrometry (LEP-OES) for long time environmental monitoring has been successfully investigated. Mechanism of decreasing channel damage by plasma discharge in microchannel of LEP for continuous elemental analysis was studied by gas introduction.

In order to study the effect of gas, new gas introduction system was designed and fabricated. The shape of micro channel was adapted from water-in-oil droplet generation. After the optimization of experimental parameters, the gas bubble can be stable generated and connected to plasma generation system. The types of gas was not shown much different properties from each other. This conclusion will be used for further mechanism investigation.

The effects of external gas introduction into AC-LEP and DC-LEP were studied. In AC-LEP, the introduction of gas into the channel resulted in the plasma starting almost immediately after the voltage was applied, while it started after several seconds without gas introduction. In both case of AC-LEP and DC-LEP, the external gas bubbles facilitated stable and high sensitive plasma generation with lower power, which result in reducing channel damage and increasing the lifetime of the analysis chip. These effects are significant in Ar introduction and AC-LEP cases. The power for homogeneous nucleation of bubble in conventional DC-LEP is higher than that required for plasma generation, resulting in high channel damage. Those facts suggest that the lower damage in conventional AC-LEP without gas introduction is attributed to H_2/O_2 bubbles generated by hydrolysis at electrodes and consequently introduced into the LEP from outside of narrow channel.

The new combination of techniques for elemental analyzer is proposed. To overcome of drawbacks of both method, an elemental analysis based on electrodeposition integration with LEP-OES has been realized. A novel configuration of reaction chamber for both electrochemical deposition and LEP detection has been developed. We investigated suitable deposition potential, solution system and working electrode materials could maintain more stable plasma and improve the intensity of deposited heavy metal ions. This system is allowed to monitoring heavy metal for a long time and continuously.

For future work, the coupled technique showed better approach for elemental analysis. We expected that this work would improve the detection sensitivity and selectivity, after further optimization. Moreover, this work might be able to detect heavy metal complex by extract metal onto working electrode, which may reduce effect from matrix, and then LEP will be used as detector.

LIST OF PUBLICATIONS

Journals

P. Ruengpirasiri, P. T. Tue, H. Miyahara, A. Okino, Y. Takamura, Study on effect of introduced gas bubbles for the low channel damage in Direct and Alternating Current Liquid Electrode Plasma Atomic Emission Spectrometry, **2019**. Jpn. J. Appl. Phys. **58**, 097001. <https://doi.org/10.7567/1347-4065/ab386b>.

International conferences

P. Ruengpirasiri, P. T. Tue, A. Okino, H. Miyahara, Y. Takamura, Improvement of channel damage and its mechanism in alternating current liquid electrode plasma atomic emission spectrometry, The Twenty Second International Conference on Miniaturized Systems for Chemistry and Life Sciences (μ TAS 2018), Kaohsiung, Taiwan, November 11-15, 2018. **(Poster presentations)**

Domestic conferences:

1. **P. Ruengpirasiri**, P. T. Tue, A. Okino, H. Miyahara, S. Tatsumi, T. Yamamoto, Y. Takamura, Effect of introduced bubbles to the generation of liquid electrode plasma by alternating current power source, The 78th JSAP Autumn Meeting, Fukuoka, September 5-8, 2017. **(Poster presentations)**
2. **P. Ruengpirasiri**, P. T. Tue, Y. Takamura, Study of the mechanism of low channel damage in AC-LEP by gas introduction, 37th CHEMINAS, Ibaraki, May 21-22, 2018. **(Poster presentations)**

3. **P. Ruengpirasiri**, P. T. Tue, H. Miyahara, A. Okino, Y. Takamura, Investigation of the mechanism of low channel damage in AC-LEP by gas introduction, The 79th JSAP Autumn Meeting, Nagoya, September 18-21, 2018. (**Poster presentations**)

Domestic Workshop:

P. Ruengpirasiri, P. T. Tue, H. Miyahara, A. Okino, Y. Takamura, Investigation of the mechanism of low channel damage in AC-LEP by gas introduction, The 2nd Excellent Core Meeting, Nomi, Japan, Dec. 4, 2018. (**Poster Presentation**)